Exosomes promote axon outgrowth by engaging the Wnt-Planar Cell Polarity pathway

Samar Ahmad[1], Melanie Pye[2], Masahiro Narimatsu[2], Siyuan Song[1], Tania Christova[1], Jeffrey L. Wrana[2], Liliana Attisano[1]

[1]Department of Biochemistry, Donnelly Centre, University of Toronto, Toronto, ON, M5S 3E1, Canada

[2]Center for Systems Biology, Lunenfeld-Tanenbaum Research Institute, Mt. Sinai Hospital and Department of Molecular Genetics, University of Toronto, Toronto, Ontario M5G 1X5, Canada

Corresponding author: liliana.attisano@utoronto.ca

Abstract

In neurons, the acquisition of a polarized morphology is achieved upon the outgrowth of a single axon from one of several neurites. Exosomes or small extracellular vesicles (sEVs) from diverse sources are known to promote the neurite outgrowth and thus may have therapeutic potential. However, the effect of fibroblast-derived exosomes on axon elongation in neurons of the central nervous system under growth permissive conditions remains unclear. Here, we show that fibroblast-derived sEVs promote axon outgrowth and a polarized neuronal morphology in mouse primary embryonic cortical neurons. Mechanistically, we demonstrate that the sEV-induced increase in axon outgrowth requires endogenous Wnts and core PCP components including Prickle, Vangl, Frizzled and Dishevelled. We demonstrate that sEVs are internalized by neurons, colocalize with Wnt7b and induce relocalization of Vangl2 to the distal axon during axon outgrowth. In contrast, sEVs derived from neurons or astrocytes do not promote axon outgrowth, while sEVs from activated astrocytes inhibit elongation. Thus, our data reveals that fibroblast-derived sEVs promote axon elongation through the Wnt-PCP pathway in a manner that is dependent on endogenous Wnts.

Introduction

Neurons are the fundamental unit of the central nervous system (CNS) and exhibit a polarized morphology comprised of a single long axon and one or multiple dendrites. Sensory signals are received by dendrites and propagated down the length of the axon to neighboring neurons (Arimura & Kaibuchi, 2007; Namba et al., 2015; Schelski & Bradke, 2017; Takano et al., 2019). Thus, proper neuronal morphology is critical for synaptic transmission and cognitive functions of the brain. To acquire a polarized morphology, one neurite outgrows the other minor neurites and forms an axon, a process referred as neuronal polarization (Arimura & Kaibuchi, 2007; Namba et al., 2015; Schelski & Bradke, 2017; Takano et al., 2019). Axons differ in their growth potential such that during development axons grow rapidly but in the adult CNS, axons have lost the ability to grow (Bradke, 2022). Hence, the study of the mechanisms of axon outgrowth during development can provide insights into processes that need to be reactivated during axon regeneration in adults. Diverse extracellular factors have been reported to modulate neurite outgrowth and neuronal morphology (Arimura & Kaibuchi, 2007; Namba et al., 2015; Schelski & Bradke, 2017; Takano et al., 2019).

Exosomes are small extracellular vesicles (sEVs) that arise from multivesicular bodies (MVBs) within the endosomal pathway. Exosomes range in size from 30-150 nm and harbor a variety of biomolecules including proteins, DNA and RNAs (Colombo et al., 2014; Pegtel & Gould, 2019; van Niel et al., 2022). Exosomes regulate many processes including immune responses, wound healing and disease pathology (Zhang et al., 2019; Yates et al., 2022; Buzas, 2023). In the CNS, exosomes act as carriers for communication among neurons and glia, and promote neuroprotective functions (Chivet et al., 2013; Bahram Sangani et al., 2021; Gassama & Favereaux, 2021; Fan et al., 2022). The biological activities of exosomes depend upon the features of the cells from which they originate. For instance, exosomes from mesenchymal stem cells increase the number of neurites and promote neurite outgrowth in cortical neurons (Xin et al., 2012; Lopez-Verrilli et al., 2016; Zhang et al., 2017) while those from Schwann cells of the peripheral nervous system (PNS) promote axon regeneration in PNS neurons (Lopez-Verrilli et al., 2013). Peripheral nerve fibroblast-derived exosomes promote Schwann cell-mediated myelination of neurons (Zhao et al., 2022). Moreover, fibroblasts promote sorting of Schwann cells at an injury site that leads to axon regrowth (Parrinello et al., 2010). Thus, both fibroblasts and Schwann cells contribute to the

remarkable regenerative ability of the PNS. In the context of growth inhibitory substrates, it has been shown that exosomes from fibroblasts can promote axon regeneration in cortical neurons (Tassew et al., 2017) suggesting that exosomes may have therapeutic potential. However, the direct effect of fibroblast-derived exosomes on axon outgrowth of CNS neurons during growth permissive conditions remains unclear. We previously showed that exosomes from fibroblasts can promote cell protrusion and motility in cancer cells (Luga et al., 2012). Given that core mechanisms of cytoskeletal remodeling are conserved during non-neuronal cell migration and neurite outgrowth in neurons, we sought to examine whether exosomes might similarly play a role in modulating neurite outgrowth. Thus, the current study is aimed at investigating the axon outgrowth promoting properties of fibroblast-derived exosomes.

Exosomes have previously been shown to mobilize autocrine Wnt-Planar cell polarity (PCP) signaling in breast cancer cells (Luga et al., 2012). PCP signaling was first described for its function in modulating tissue polarity by aligning cells in a single plane, perpendicular to the apical-basal axis (Goodrich & Strutt, 2011; Yang & Mlodzik, 2015; Devenport, 2016; Koca et al., 2022). In vertebrates, PCP signaling also functions in the development of inner ear, orientation of hair follicles and convergent extension (CE) movements during gastrulation and neural tube closure (Jones & Chen, 2007; Wallingford, 2012; Butler & Wallingford, 2017; Davey & Moens, 2017; Wang et al., 2019; Montcouquiol & Kelley, 2020). In the CNS, PCP modulates numerous developmental processes including differentiation of neural progenitor cells, neuronal migration, axon guidance and dendritic arborization (Goodrich, 2008; Davey & Moens, 2017; Hakanen et al., 2019; Zou, 2020). Core components of the PCP pathway are the seven-pass transmembrane Frizzled (Fzd) receptors, four-pass transmembrane Van-Gogh-like (Vangl) proteins, and cytoplasmic proteins including Prickle (Pk) and Dishevelled (Dvl) (Goodrich & Strutt, 2011; Yang & Mlodzik, 2015; Devenport, 2016; Koca et al., 2022). Unlike in Drosophila, Wnt morphogens play an important role in regulating PCP signaling in vertebrates, and may act as an instructive cue (Butler & Wallingford, 2017).

Wnts are lipid-modified secreted glycoproteins that act as morphogens to regulate processes during embryonic development including cell proliferation and fate, polarity and migration (Willert & Nusse, 2012; Nusse & Clevers, 2017; Steinhart & Angers, 2018; Mittermeier & Virshup, 2022;

103 Rim et al., 2022). In neurons, Wnts are known to modulate dendritogenesis, axon guidance and
104 remodelling, synaptogenesis, synaptic plasticity and differentiation (Salinas, 2012; Bonansco et
105 al., 2022). In mammals, there are 19 Wnts that bind to different classes of cell surface receptors
106 and trigger diverse cellular responses (Rim et al., 2022). Wnt receptors and co-receptors include
107 members of Fzd, low-density lipoprotein related receptor (LRP) and receptor tyrosine kinases
108 (RTKs) such as ROR, RYK, and PTK7 (MacDonald & He, 2012; Niehrs, 2012). Despite
109 increasing knowledge about Wnt signaling, little is known about the role of Wnt-PCP pathway in
110 axon outgrowth.
111
112 The current study was aimed at investigating the contribution of Wnt-PCP signaling in exosome-
113 induced axon outgrowth. We show that sEVs derived from diverse fibroblast cell lines promote
114 axon outgrowth that leads to acquisition of a polarized neuronal morphology. Mechanistically, we
115 show that the sEV-induced increase in axon outgrowth requires neuronally-expressed Wnts and
116 PCP components including Pk, Vangl, Fzd and Dvl. Importantly, we show that sEVs are
117 internalized by neurons where they can colocalize with Wnt7b and also induce a shift in Vangl2
118 localization towards distal part of axon. In contrast to fibroblast-derived sEVs, those isolated from
119 neurons or astrocytes do not alter axon outgrowth, while sEVs isolated from activated astrocytes
120 inhibit axon outgrowth. Overall, the current study uncovers the potential of fibroblast-derived
121 sEVs in activating axon outgrowth systems through PCP signaling, and may also indicate the
122 therapeutic potential of sEVs in treating neuronal injury.
123
124 **Results**
125 **sEVs promote acquisition of a polarized neuronal morphology by enhancing axon outgrowth**
126 Dissociated primary mouse embryonic cortical neurons when freshly plated *in vitro* (Fig. S1A)
127 give rise to short neurites, one of which grows rapidly to form an axon by 24-48 hours to generate
128 a polarized neuron (Dotti et al., 1988; Arimura & Kaibuchi, 2007). Recent studies have
129 demonstrated that exosomes isolated from mesenchymal stem cells can promote neurite outgrowth
130 (Lopez-Verrilli et al., 2016; Zhang et al., 2017). Thus, we sought to explore the role of fibroblast
131 derived EVs in neurite outgrowth. Following the guidelines of International Society for
132 Extracellular vesicles (ISEV) (Welsh et al., 2024), the isolated vesicles are hereafter referred as
133 sEVs, instead of exosomes. We first isolated and characterized sEVs from diverse mouse and

134 human fibroblast cell culture supernatants including mouse L cells, mouse embryonic fibroblasts
135 (MEFs), human dermal fibroblasts (HDFn), normal human lung fibroblasts (NHLF) and BJ
136 foreskin fibroblasts using differential centrifugation (Fig. 1A). Analysis of the final pellet by
137 immunoblotting revealed the presence of EV markers CD81, TSG101 and Flotillin1, and the
138 absence of the endoplasmic reticulum (ER)-resident protein, Calnexin (CNX) (Fig. 1B). Particle
139 size distribution analysis of the final pellet using nanoparticle tracking analysis (NTA) showed
140 that the majority of particles were within a size range of 30-150 nm (Fig. 1C) that is characteristic
141 of exosomes or sEVs (Colombo et al., 2014). Ultrastructural analysis by transmission electron
142 microscopy (TEM) further showed intact round vesicles ranging in sizes of 30-150 nm in diameter,
143 thus, confirming the identity and structural integrity of the isolated sEVs (Fig. 1D).
144
145 We next investigated the role of the fibroblast-derived sEVs on the neuronal morphology using
146 dissociated E15.5 – 16.5 primary mouse embryonic cortical neurons. Neurons were treated 4 h
147 after plating with sEVs for either 20 or 29 hours and were fixed and stained with Tuj1 antibody,
148 which detects the neuron specific β-III tubulin. Quantification of neurite lengths revealed that
149 sEVs from all five fibroblast lines enhanced the length of the longest neurite (ie the prospective
150 axon) from a median length of ~30 μm (in controls) to ~60 μm at 24 h and from ~40 μm (in
151 controls) to ~75 μm at 33 hours (Fig. 1E and 1F). In contrast, the individual lengths (~10 μm) and
152 the total combined length (~20 μm) of the remaining neurites, excluding the longest, referred to as
153 minor neurites and correspond to prospective dendrites, remained either unchanged or slightly
154 reduced (Fig. 1G and 1H). The total number of neurites was also unaltered by sEV treatment (Fig.
155 1I). Similarly, when neurons were treated with varying concentrations of sEVs (0.05-10 μg/mL)
156 obtained from all five fibroblast cell lines, a dose-dependent increase in the length of the longest
157 neurite at both 24 and 33 hours was observed with the maximal effect occurring at 5 μg/mL (Fig.
158 S1B-K). To verify that sEVs preferentially act on axons, neurons treated with sEVs from L cells
159 were co-stained with the axonal marker, Tau-1 and the dendritic marker, MAP2. Quantification
160 of Tau-1 positive axons confirmed that sEVs increased the length of axons (Fig. S2A and S2B),
161 yielding results similar to those obtained when the length of the longest neurite, independent of
162 Tau-1 staining was quantified in parallel (Fig. S2C). Similar to the data observed in Fig. 1G, the
163 length of individual neurites (~10 μm) positive for the dendritic marker MAP2 was either
164 unaffected or slightly reduced by sEVs (Fig. S2D). Moreover, sEV treatment concordantly resulted

165 in a significant increase in the percent of neurons with Tau-positive axons, a characteristic of a
166 polarized neuron that was clearly evident within 24 h of plating (Fig. S2E). Importantly, the
167 increase in the percent of Tau-positive axons could be observed as early as 12 hours after plating,
168 indicating the rapid effect of sEVs (Fig. S2F and S2G). Taken together, these results demonstrate
169 that sEVs derived from a variety of fibroblast lines, promote axon outgrowth and accordingly
170 enhance the acquisition of a polarized phenotype.
171
172 The sEV-induced increase in axon outgrowth was lost when sEVs were incubated with detergent,
173 which causes lysis of sEVs (Cvjetkovic et al., 2016; Bonsergent et al., 2021) or upon treatment
174 with Proteinase K which digests surface accessible proteins (Fig. S3A and S3B). This indicates
175 that while the axon-promoting activity is not found inside the sEVs, intact sEVs are required for
176 function, suggesting that the active proteins might be expressed on the surface of sEVs. Next, to
177 rule out a potential role for contaminating cell membranes or protein aggregates in mediating the
178 effects on neuronal morphology, we undertook two different and more stringent exosome isolation
179 protocols, where the final ultracentrifugation (100,000 x g) pellet of sEVs obtained from L cell
180 supernatants was further subjected to either density gradient purification (Fig. S3) or size exclusion
181 chromatography (Fig. S4). For density gradient separation, the resuspended pellet was applied to
182 a discontinuous iodixanol gradient and then subjected to an additional ultracentrifugation (Fig.
183 S3C). Characterization of the floating fractions by immunoblotting demonstrated that Fractions 6
184 – 8 were positive for the EV markers, CD81 and Flotillin1 (Fig. S3D) with the intensity of both
185 markers peaking in Fraction 7 (Fig. S3E). Of note, Fraction 9 had the highest amount of total
186 protein but very low levels of EV markers (Fig. S3E) indicating a successful enrichment of EV
187 particles in Fractions 6 - 8. Particle size distribution analysis showed that the number of particles
188 peaked at approximately 100 nm, which is a characteristic of exosomes or sEVs, and that Fraction
189 7 had the highest number of particles (Fig. S3F). Moreover, Fraction 7 (F7) had the highest
190 particle/protein ratio (Fig. S3G), a parameter that is widely used to measure the purity of EVs
191 (Webber & Clayton, 2013; Thery et al., 2018). Treatment of dissociated neurons with these
192 purified sEVs from the F7 fraction revealed that the length of the longest neurite (ie the prospective
193 axon) was increased to levels similar to that observed for the initial ultracentrifugation pellet
194 (sEVs) at all time points (Fig. S3H and S3I).
195

196 Next, we used size exclusion chromatography as an alternative approach to purify sEVs from the
197 ultracentrifugation (100,000 x g) pellets (Fig. S4A). Characterization of the isolated fractions
198 revealed the presence of the EV markers, CD81, Flotillin1 and Tsg101 but not the ER protein,
199 Calnexin (CNX) in fractions 7 – 12 (Fig. S4B), with particle size peaking at a diameter of
200 approximately 100 nm with fraction F7 having the highest particle/protein ratio (Fig. S4C and D)
201 which is characteristic of exosomes or sEVs. Treatment of dissociated neurons with F7 purified
202 sEVs revealed that the length of the longest neurite (ie the prospective axon) was increased to
203 levels similar to that observed for the initial ultracentrifugation pellet (sEVs) at both 24 and 33
204 hours (Fig. S4E and S4F) as observed previously (Fig. 1E, 1F and S1). Of note, outgrowth induced
205 by sEVs isolated using either purification method was easily detected as early as 12 hours (ie 8 h
206 after sEV addition), highlighting the rapid nature of the response (Fig. S3H, S3I, S4E and S4F).
207
208 Altogether, these observations suggest that the sEVs isolated by ultracentrifugation (100,000 x g
209 pellet) are responsible for promoting axon outgrowth. Since the responses induced by these
210 pelleted sEVs were similar to that achieved after more extensive purifications, we used this
211 ultracentrifuged pellet as a source of sEVs for all subsequent experiments.
212
213 **The PCP pathway is required for sEV-induced growth of the prospective axon**
214 Previous work has demonstrated that in cancer cells, motility induced by exogenously added
215 fibroblast-derived exosomes is mediated by the Wnt planar cell polarity pathway (PCP) in recipient
216 cells (Luga et al., 2012). Prickle (Pk) and Vangl, core PCP components, distribute asymmetrically
217 to the proximal side in planar polarized epithelial cells (Yang & Mlodzik, 2015; Butler &
218 Wallingford, 2017) and are also known to modulate neuronal morphology (Dreyer et al., 2022;
219 Radaszkiewicz et al., 2023). This prompted us to investigate whether core PCP components might
220 be required for sEV-induced axon outgrowth. To study this, we used a combination of siRNA-
221 mediated knockdown and mouse genetic models to explore the role of these core PCP components
222 in dissociated primary cortical neurons. There are two Prickle genes, Prickle 1 and Prickle 2 (Pk1
223 and Pk2), expressed in cortical neurons (Fig. S5A). To test for the requirement for Prickle, neurons
224 were co-transfected with siRNAs targeting Pk1 and/or Pk2 along with plasmid, encoding GFP to
225 visualize transfected cells. Analysis of GFP positive neurons in which expression of Pk1 and Pk2
226 alone or together was abrogated, revealed that neurons were comprised solely of minor neurites

227 (mean length ~10 μM), none of which were elongated upon treatment with sEVs (Fig. 2A and 2B).
228 Knockdown efficiency was confirmed by qPCR after FACS sorting for GFP positive neurons (Fig.
229 2C). As an alternative to this transient approach, we explored the consequences on neuronal
230 morphology using dissociated neurons isolated from mice with genetic loss of Pk1 or Pk2. While
231 Pk2 knockout mice are viable (Tao et al., 2011), Pk1 knockout mice display early embryonic
232 lethality (Tao et al., 2009). Thus, we generated mice with single floxed Pk alleles ($Pk1^{f/f}$ and $Pk2^{f/f}$)
233 using targeted homologous recombination (Fig. S5B), which were then crossed with each other to
234 obtain mice with double ($Pk1^{f/f}$;$Pk2^{f/f}$) floxed Pk alleles. Both single and double floxed mice, after
235 removal of neomycin cassette, were viable, fertile, and exhibited no overt anatomical defects.
236 Conditional knockout mice were then generated by crossing with Nestin-Cre mice to achieve loss
237 of Pk1/2 in the developing brain. Loss of Pk1/2 expression in the cortex of $Pk1^{f/f}$;$Pk2^{f/f}$;Nestin-Cre
238 E15.5 embryos was confirmed by immunofluorescence microscopy using Pk1 and Pk2 antibodies
239 (Fig. S5C and S5D). Consistent with the siRNA results, analysis of cortical neurons (E15.5-16.5)
240 isolated from mice with a Nestin-Cre conditional deletion of either Pk1 alone, Pk2 alone or both
241 ($Pk1^{f/f}$;$Pk2^{+/+}$;Nestin-Cre, $Pk1^{+/+}$;$Pk2^{f/f}$;Nestin-Cre or $Pk1^{f/f}$;$Pk2^{f/f}$;Nestin-Cre, respectively)
242 revealed the presence of only short neurites that failed to elongate in response to sEV treatment in
243 contrast to the $Pk1^{+/+}$;$Pk2^{f/f}$ or $Pk1^{+/+}$; $Pk2^{+/+}$;Nestin-Cre controls (Fig. 2D and S5E).
244
245 We next explored the contribution of the core PCP tetraspanin proteins, Vangl1 and Vangl2, which
246 regulate diverse aspects of neuronal development (Dreyer et al., 2022). Abrogation of Vangl2
247 expression using siRNAs strongly decreased sEV-mediated induction of outgrowth of the longest
248 neurite (Fig. 2E-G). Interestingly, in the case of siVangl1, while the length of the longest neurite
249 was reduced, sEVs maintained the ability to promote elongation (Fig. 2E-G), suggesting that
250 Vangl2, but not Vangl1 is important for the sEV-mediated effects. Loop-tail mice harbor a S464N
251 point mutation in the Vangl2 allele (Kibar et al., 2001; Murdoch et al., 2001) that results in reduced
252 Vangl2 protein levels and defective translocation to plasma membrane (Torban et al., 2007; Merte
253 et al., 2010; Belotti et al., 2012). Morphological examination showed that the heterozygous loop-
254 tail embryos ($Vangl2^{+/Lp}$) exhibited a curly tail with partial or no neural tube defects, whereas
255 homozygous loop-tail embryos ($Vangl2^{Lp/Lp}$) exhibited a completely open neural tube (Fig. 2H) as
256 previously reported (Kibar et al., 2001). Consistent with the siRNA results, dissociated cortical
257 neurons isolated from E15.5 – 16.5 $Vangl2^{Lp/Lp}$ embryos, but not wild-type or heterozygotes (Lp/+)

258 displayed short neurites (~ 10 μM in length) and a loss of sEV-induced outgrowth of the longest
259 neurite at both 24 and 33 hours (Fig. 2I and S5F).
260
261 Smurf1 and Smurf2 are E3 ubiquitin ligases that modulate PCP signaling to control convergent
262 extension, cell protrusion and motility (Wang et al., 2003; Sahai et al., 2007; Narimatsu et al.,
263 2009; Luga et al., 2012) and have also been shown to play a key role in regulating neuronal
264 morphology (Vohra et al., 2007; Cheng et al., 2011; Kannan et al., 2012). Since cortical neurons
265 express both Smurf1 and Smurf2 as determined by RNA sequencing analysis (Fig. S5A), we next
266 explored whether Smurfs might have a role in sEV-induced axon outgrowth. For this, we
267 examined the contribution of Smurf1 and/or Smurf2 using dissociated neurons isolated from Smurf
268 knockout mice. Smurf1$^{+/-}$;Smurf2$^{+/-}$ double heterozygotes (Narimatsu et al., 2009) were crossbred
269 to generate offspring with varying Smurf1/2 genotypes. Analysis of dissociated cortical neurons
270 revealed that complete loss of either Smurf1 alone (Smurf1$^{-/-}$; Smurf2$^{+/+}$) or Smurf2 alone
271 (Smurf1$^{+/+}$;Smurf2$^{-/-}$) yielded neurons that harboured only short neurites (~ 10 μM in length) and
272 that sEV-induced outgrowth of the longest neurite was prevented in contrast to wild-type or
273 heterozygote (Smurf1$^{+/-}$;Smurf2$^{+/-}$) littermates (Fig. S5G and S5H). These results suggest that
274 Smurf1 and Smurf2 act in a non-redundant manner or that a minimal level of combined Smurf1/2
275 activity is required for neurite outgrowth.
276
277 Both PCP and canonical β–catenin signaling is initiated upon binding of Wnt ligands to one of 10
278 members of the seven-pass transmembrane Frizzled family of receptors (Fzd) and is then
279 propagated intracellularly through one of three Dishevelleds (Dvls) (van Amerongen et al., 2008;
280 Gao & Chen, 2010; MacDonald & He, 2012; Yang & Mlodzik, 2015; Wang et al., 2016; Sharma
281 et al., 2018). Thus, we next explored which Fzds and Dvls are required for sEV-mediated axon
282 outgrowth. Cortical neurons treated with a pan-Fzd blocking antibody (F2.A) that recognizes
283 multiple Fzds, including Fzd1, 2, 4, 5, 7 and 8 (Pavlovic et al., 2018; Tao et al., 2019) displayed
284 only minor neurites that failed to elongate in response to sEVs (Fig. 3A and 3B). Treatment of
285 cortical neurons with F2.A at a later time point had no effect on the axon length, however, the
286 sEV-induced increase in the axon length was impaired, indicating that Fzds are required to mediate
287 sEV effects (Fig. S6A and S6B). Mouse E15.5-16.5 cortical neurons express Fzd1, 2, 3, 7, 8 and
288 9 with Fzd1 and Fzd3 displaying the highest levels (Fig. S5A), thus we next explored the individual

289 requirement for these receptors using siRNAs. Quantification revealed that individual loss of Fzd1,
290 3 or 9 yielded neurons with minor neurites that failed to elongate in response to sEVs while loss
291 of Fzd7 only blocked sEV-mediated outgrowth (Fig. 3C, S6C and S6D). Loss of Fzd2 or Fzd8 had
292 no effect, though equivalent knockdown efficiency was achieved (Fig. S6D). These results indicate
293 that multiple but specific Fzds (Fzd 1, 3 and 9) are required for basal elongation, whereas only
294 Fzd7 is specifically required for sEV-mediated outgrowth of the prospective axon. All three
295 Dishevelleds (Dvl1, 2 and 3) are expressed in cortical neurons with Dvl1 being expressed at the
296 highest level (Fig. S5A). Analysis of the requirement for Dvls using siRNAs revealed that only
297 Dvl2 was required for sEV-induced outgrowth (Fig. 3D, S7A and S7B).
298
299 Individual Fzds and Dvls function in both PCP and β-catenin pathways in a complex and highly
300 redundant manner thus it is challenging to associate specific Fzds/Dvls to a particular pathway
301 (Gao & Chen, 2010; Mlodzik, 2016; Wang et al., 2016). However it is worth noting that evidence
302 of Fzd7 and Dvl2, both of which we observed to be specifically required for sEV-induced growth
303 of the prospective axon, have been reported to function in PCP pathways (Zou, 2020; Pascual-
304 Vargas & Salinas, 2021). Taken together, these observations suggest that core PCP components
305 are required for basal neurite elongation and that they are required for sEV-induced growth of the
306 longest neurite.
307
308 **Vangl2 localizes asymmetrically during sEV-induced growth of the longest neurite**
309 Prior work has revealed that Wnt5a-mediated activation of the PCP pathway in dissociated
310 commissural neurons results in relocalization of Vangl2 to the growth cone (Shafer et al., 2011).
311 Thus, we next explored whether sEVs might similarly promote relocalization of Vangl2. In control
312 (PBS) or sEV-treated embryonic cortical neurons, Vangl2 was distributed in both the somal
313 membrane and in the axon but in distinct patterns (Fig. 3E). Quantification of Vangl2 distribution
314 within the axon shaft revealed that in controls, a preferential localization in the proximal half of
315 the axon was observed (Fig. 3F), that was independent of axon length (Fig. S7C). Remarkably, in
316 neurons treated with sEVs for 20 h, Vangl2 relocalized to the distal end of the axon (distal to
317 proximal intensity ratio of ~1.6 versus ~0.6 in controls) and was often detected within the growth
318 cone (Fig. 3F). No overt change in Vangl2 localization in the somal membrane was observed. This

319 re-localization of Vangl2 to the distal axon and growth cone suggests that sEVs engage PCP
320 components to promote axon growth.
321
322 **Neuronal Wnts mediate sEV induced growth of the longest neurite**
323 Wnts, including Wnt5a, Wnt7a and Wnt7b can promote axon elongation, neurogenesis and axon
324 guidance, respectively, via the PCP pathway (Salinas, 2012; Bonansco et al., 2022). As exosomes
325 are known to carry Wnts (Routledge & Scholpp, 2019; Gross, 2021; Mittermeier & Virshup,
326 2022), we next explored whether the presence of Wnt ligands in isolated exosomes could
327 contribute to the observed outgrowth of neurites. We first abrogated the expression of Porcupine,
328 an acyltransferase essential for Wnt lipidation and secretion (Mikels & Nusse, 2006; Takada et al.,
329 2006), in the exosome-producing L cells using siRNAs and isolated the sEVs (Fig. 4A).
330 Abrogation of Porcupine expression had no effect on the overall number of sEVs secreted or on
331 the levels of the EV markers, CD81, Flotillin1 and TSG101 as indicated by immunoblotting (Fig.
332 S7D-G). Moreover, ultrastructural analysis by TEM revealed intact round, exosome-like vesicles
333 in both the control and Porcupine knockdown samples (Fig. S7H). When applied to cortical
334 neurons, sEVs isolated from Porcupine-deficient L cells were as active as control sEVs in
335 promoting outgrowth of the longest neurite (Fig. 4B-D). Immunodetection of endogenous Wnt
336 proteins in wild type L-cells is challenging, thus we confirmed that siPorcupine inhibits Wnt
337 secretion using L-cells stably expressing Wnt5a (Fig. S7I-K). These results thereby indicate that
338 the activity of L cell-derived sEVs was not due to the presence of Wnts within the sEVs.
339
340 We next sought to determine whether L cell-secreted exosomes might modulate autocrine Wnt
341 signaling, a process whereby secreted Wnts bind to cell-surface receptors and thereby activate Wnt
342 signaling in neurons to promote neurite outgrowth. To investigate this, we blocked the ability of
343 neurons to secrete Wnts, thus attenuating the autocrine signaling, by chemically inhibiting the
344 activity of Porcupine using IWP2 or LGK974 (Chen et al., 2009; Liu et al., 2013) (Fig. 4E). As
345 endogenous Wnt proteins are difficult to detected in neurons, we confirmed that IWP2 blocked
346 Wnt secretion using L-Wnt5a cells (Fig. S7L) as described above for siPorcupine (Fig. S7-I-K).
347 We observed that treatment of cortical neurons with Porcupine inhibitors 4 h after plating,
348 prevented sEV-mediated neurite outgrowth (Fig. 4F and G). In contrast, treatment with IWP2 at
349 24 h after plating, had no effect on basal axon lengths but impaired the sEV-induced axon

350 outgrowth, thus indicating that neuronal Wnts are required to mediate the effect of sEVs (Fig. S8A
351 and S8B). The Wnt carrier protein, Wntless (Wls) is required for Wnt secretion (Banziger et al.,
352 2006), and abrogating expression of Wls using siRNAs, similarly prevented sEV-induced neurite
353 outgrowth (Fig. 4H-J). Thus, blocking pathways essential for Wnt secretion prevents sEV-induced
354 growth of the longest neurite, indicating that neuronally-expressed endogenous Wnts are necessary
355 for sEV function.
356
357 Analysis of RNA sequencing results revealed that cortical neurons express Wnt5a, Wnt5b, Wnt7a
358 and Wnt7b (Fig. S5A). We verified by qPCR that these Wnts were expressed in neurons and that
359 expression levels remain constant throughout the time frame of the experiment (Fig. S8C). Thus,
360 to determine which Wnts are important for neurite outgrowth, the expression of each Wnt was
361 individually abrogated using siRNAs (Fig. S8D). Neurons lacking Wnt5b, Wnt7a or Wnt7b but
362 not Wnt5a were comprised solely of minor neurites, none of which elongated upon treatment with
363 sEVs (Fig. 4K and 4L). Altogether, these observations suggest that exogenously added sEVs might
364 engage endogenous Wnts (Wnt5b, Wnt7a and Wnt7b) to promote growth of the longest neurite.
365
366 **sEVs associate with Wnts during neurite outgrowth**
367 To explore sEV uptake in neurons, we used a compartmentalized microfluidic chamber device
368 (Taylor et al., 2005) comprised of a set of proximal compartments, where neurons are seeded, and
369 a set of distal compartments where axons emerge. The compartments are connected by a
370 microgroove barrier that enables a gradient based fluidic separation due to the hydrostatic pressure
371 (Fig. 5A). Plated neurons were grown for 5 days to allow axons to reach the distal compartment.
372 sEVs were added to either compartment for 24 hours and then neurons were fixed and stained for
373 Tuj1. Addition of sEVs to the proximal compartment containing the cell bodies but not to the distal
374 compartment containing axon tips, promoted elongation of neurites (Fig. 5B and 5C).
375
376 To directly visualize sEV uptake, we used conditioned media (CM) from L cells stably expressing
377 CD81-EYFP as a source of EYFP-labelled sEVs (Luga et al., 2012). Immunoblotting of both the
378 conditioned media (CM) and the sEV pellet revealed the presence of EYFP using an anti-GFP
379 antibody (Fig. 5D and 5E), indicating successful integration of the CD81-EYFP fusion protein in
380 sEVs. Neurons were treated with the CM from either control or CD81-EYFP expressing L cells

381 for 29 hours. Immunostaining followed by confocal microscopy revealed that the majority of GFP-
382 positive neurons displayed abundant GFP puncta within the soma as well as occasional staining in
383 the axon, suggesting that sEVs were internalized (Fig. 5F). Next, neurons were incubated with CM
384 containing CD81-EYFP-labelled sEVs for 30 minutes, washed and subsequently chased in regular
385 CM media for varying times prior to fixation. We found that sEVs were internalized by neurons
386 within the 30 min exposure time, and that the internalized sEVs were found both in the soma and
387 in axons throughout the time course (0 - 24 hours) (Fig. S8E). Thus, sEVs are rapidly (within 30
388 min) taken up by neurons and can be detected as long as 24 h later.
389
390 In cancer cells, internalized exosomes acquire endogenous Wnts to activate PCP signaling (Luga
391 et al., 2012). Given that sEVs were internalized in neurons, we next investigated whether the
392 internalized sEVs could associate with the Wnts. Cortical neurons were electroporated with HA-
393 tagged Wnt7b (Wnt7b-HA) or empty vector control and 24 hours after plating were treated with
394 EYFP-labelled sEVs for 30 min. Immunostaining with anti-HA and GFP antibody showed
395 colocalization of Wnt7b-HA and sEVs in the soma (Fig. 5G and 5H). Next, we examined whether
396 exosomes were colocalized with endogenous Wnt7b, the ligand most highly expressed in neurons.
397 Neurons were treated with 10X concentrated CM obtained from either control or CD81-EYFP
398 expressing L cells for 30 min and then were fixed and immunostained with anti-GFP and anti-
399 Wnt7b antibodies, whose specificity was first confirmed by immunofluorescence microscopy (Fig.
400 S8F). This analysis revealed colocalization of Wnt7b and sEVs in both the soma and axon (Fig. 5I
401 and 5J). Given that internalized sEVs colocalize with Wnt7b, and that endogenous Wnts are
402 required for sEV-induced outgrowth, our findings suggest that internalized sEVs may acquire
403 neuronally expressed Wnt7b to promote axon outgrowth.
404
405 **sEVs from neurons and astrocytes do not promote neurite outgrowth**
406 In the brain, exosomes mediate glia-neuron communication during developmental processes and
407 pathogenesis (Chivet et al., 2013; Bahram Sangani et al., 2021; Gassama & Favereaux, 2021; Fan
408 et al., 2022). Neurons and astrocytes are the two major cell types in the CNS, and are known to
409 secrete exosomes (Gassama & Favereaux, 2021). Thus, we sought to determine whether exosomes
410 released from neurons or astrocytes also modulate neurite outgrowth. To examine this, we first
411 isolated and tested sEVs produced by primary embryonic cortical neurons (Fig. 6A). sEV pellets

412 were positive for EV markers and displayed the typical 30-150 nm diameter size range (Fig. S9A
413 and S9B). However, in contrast to fibroblast-derived sEVs, these sEVs did not promote neurite
414 outgrowth when added to neurons at any dose tested, including at concentrations much higher
415 (0.05-10 μg/mL) than those required for fibroblast-derived sEV effects (Fig. 6B and C). Thus,
416 sEVs exogenously secreted from neurons do not promote neurite outgrowth.
417
418 Astrocytes support many physiological functions of neurons including synapse development and
419 neuronal activity, whereas reactive astrocytes produced during injury or aging (Clarke et al., 2018)
420 contribute to the production of the inhibitory environment that prevents axon regeneration (Clarke
421 & Barres, 2013; Pekny & Pekna, 2014; Liddelow & Barres, 2017; Lee et al., 2022). Thus, we next
422 investigated the role of astrocyte-derived exosomes on neurite outgrowth (Fig. 6A). For this, we
423 isolated primary mouse astrocytes from newborn pups at postnatal day (P) 1-4 and confirmed their
424 identity by positive staining for GFAP (Fig. S9C) and negative staining for the neuronal marker,
425 Tuj1 (Fig. S9C). Reactive astrocytes were generated by treating isolated astrocytes with bacterial
426 lipopolysaccharide (LPS), which induced upregulation of the expression of proinflammatory
427 cytokines including TNF-α, iNOS-2, IL-1β and IL-6 as determined by qPCR (Fig. S9D),
428 confirming astrocyte activation. sEVs were purified from control and LPS-activated astrocytes
429 using differential centrifugation and the presence of sEVs in pellets confirmed by immunoblotting
430 for CD81, TSG101 and Flotillin1 and by confirming particle diameters using NTA (Fig. S9E and
431 S9F). Interestingly, treatment of neurons with varying doses of sEVs isolated from either control
432 or LPS-activated astrocytes inhibited neurite outgrowth (Fig. 6D-G). As tissue culture plastic is
433 much stiffer than the normal *in vivo* environment and can stimulate partial activation of astrocytes
434 (East et al., 2009), we next cultured astrocytes in a soft 3D-collagen gel, hereafter referred as 3D-
435 astrocytes. GFAP expression is higher in activated astrocytes (Escartin et al., 2021) and
436 accordingly, astrocytes grown on a 2D-plastic surface showed much higher GFAP staining as
437 compared to those cultured in the 3D-collagen gel (Fig. S9G). Moreover, treatment of 3D-
438 astrocytes with LPS, enhanced GFAP expression (Fig. S9H). Next, sEVs were isolated from
439 control and LPS-activated 3D-astrocytes and were confirmed to display typical exosome size using
440 NTA (Fig. S9I-K). Remarkably, sEVs isolated from 3D-astrocytes had no effect on the neurite
441 outgrowth (Fig. 6H and I), whereas sEVs from LPS-activated 3D-astrocytes inhibited the neurite
442 outgrowth (Fig. 6J and K). Thus, our results indicate that while reactive astrocytes inhibit neurite

443 outgrowth, control, unstimulated astrocytes grown in a soft environment do not alter neuronal
444 morphology.
445
446 Taken together, these findings suggest that fibroblast-derived sEVs can promote neurite
447 outgrowth, and this ability is not a general property of sEVs. Collectively, the data supports a
448 model in which sEVs engage Wnt-PCP signaling in neurons to promote axon outgrowth and a
449 polarized morphology. We suggest a novel mechanism whereby internalized sEVs which co-
450 localize with Wnt ligands, such as Wnt7b, induce relocalization of the core PCP component,
451 Vangl2 from the soma to distal part of the axon and thereby promote axon outgrowth (Fig. 7).
452
453
454 **Discussion**
455 Exosomes are increasingly being studied for therapeutic applications (Dai et al., 2020; Kalluri &
456 LeBleu, 2020). Exosomes from diverse sources are shown to modulate neurite outgrowth, but how
457 fibroblast-derived exosomes act to specifically affect neuronal morphology remains unclear. Here,
458 we show that fibroblast-derived sEVs can engage Wnt-PCP signaling in neurons and thereby
459 promote axon outgrowth and acquisition of a polarized neuronal morphology. We demonstrate
460 that sEVs are internalized via the soma in neurons and can colocalize with endogenous Wnt7b and
461 that sEVs induce relocalization of the core PCP component, Vangl2 to the distal region of the
462 axon. Thus, our work demonstrates that sEVs can engage Wnt-PCP signaling in neurons to
463 promote axon outgrowth.
464
465 Exosomes derived from diverse sources harbour the ability to promote axon or dendrite elongation.
466 For instance, exosomes from Schwann cells of the PNS have been shown to promote neurite
467 outgrowth in dorsal root ganglia (DRG) neurons, and exosomes from mesenchymal cells enhance
468 neurite outgrowth in DRG and CNS-derived cortical neurons (Xin et al., 2012; Lopez-Verrilli et
469 al., 2013; Lopez-Verrilli et al., 2016; Zhang et al., 2017). In the case of fibroblasts, exosomes from
470 these cells can promote neurite outgrowth in DRG neurons in normal, uninjured contexts, and can
471 enhance axon regeneration in injured sciatic nerves (Zhao et al., 2023). In addition, fibroblasts can
472 promote Schwann cell migration and sorting, both of which are associated with axonal regrowth
473 (Dreesmann et al., 2009; Parrinello et al., 2010; van Neerven et al., 2013). In our study, we found

474 that fibroblast-derived sEVs can promote axon outgrowth in cortical neurons and that they act
475 through the Wnt-PCP pathway. In contrast, in a prior study, fibroblast-derived exosomes were
476 shown to promote axon regeneration in a Wnt-dependent manner but did so via the mTOR pathway
477 and only in neurons grown in an inhibitory environment (Tassew et al., 2017). Thus, exosomes
478 appear to be capable of activating distinct neuronal signaling pathways in growth permissive
479 versus inhibitory contexts. In contrast to fibroblasts, we observed that sEVs derived from primary
480 neurons or unactivated astrocytes had no effect on neurite outgrowth even when used at higher
481 concentrations. Upon damage, activated astrocytes contribute to the inhibitory microenvironment
482 by forming a glial scar at the injury site (Pekny & Pekna, 2014; Liddelow & Barres, 2017; Lee et
483 al., 2022). In line with this, we observed that sEVs derived from LPS-activated astrocytes inhibit
484 neurite outgrowth, which is consistent with a previous report showing that exosomes from
485 Interleukin-1β-activated human primary astrocytes similarly inhibited neurite outgrowth in mouse
486 cortical neurons (You et al., 2020). This suggests that the cell type and state of exosome secreting
487 cells determines the axon growth promoting properties of exosomes. Understanding the
488 mechanisms that alter exosome cargos to thereby modulate the effects on neurons is an important
489 area for future investigation.
490
491 Core PCP components modulate many aspects of neuronal morphology including neuronal
492 polarization, axon outgrowth, axon guidance and synapse formation (Goodrich, 2008; Davey &
493 Moens, 2017; Hakanen et al., 2019; Zou, 2020). Our data shows that both of the related PCP
494 components, Pk1 and Pk2 are required for growth of the prospective axon, which is consistent with
495 a recent study showing that Pk2 is necessary for proper neuronal polarity in rat hippocampal
496 neurons (Dorrego-Rivas et al., 2022). We also observed that the absence of Pk1 and Pk2 attenuated
497 sEV-induced growth of the longest neurite. Another core PCP component, Vangl2 has been
498 reported to exhibit differential effects in distinct neurons. For instance, downregulation of Vangl2
499 in commissural neurons using shRNAs inhibited Wnt5a-induced axonal outgrowth (Shafer et al.,
500 2011), whereas hippocampal neurons from Vangl2 conditional-knockout mice exhibited increased
501 basal and Wnt5a-induced axon outgrowth (Dos-Santos Carvalho et al., 2020). In our study, we
502 observed that both Vangl1 and Vangl2 are required for basal neurite outgrowth and that only
503 Vangl2 is required for sEV-induced neurite outgrowth. Importantly, sEVs induced relocalization
504 of Vangl2 to the distal part of the axon, further supporting a role for Vangl2 in sEV-mediated axon

505 outgrowth. Although not designated as core PCP components, members of the Smurf E3 ubiquitin
506 ligase family are important regulators of PCP, and can modulate neuronal morphology (Vohra et
507 al., 2007; Narimatsu et al., 2009; Cheng et al., 2011; Kannan et al., 2012). Consistently, we found
508 that both Smurf1 and Smurf2 are required for neurite outgrowth, and that sEV-induced neurite
509 outgrowth is attenuated in Smurf1 and Smurf2 knockout neurons. Taken together, these results
510 demonstrate that sEVs engage key components of the Wnt/PCP pathway to modulate
511 neuritogenesis.
512
513 Fzd receptors and Dvls are essential for PCP signaling, but also mediate canonical Wnt/β-catenin
514 signals (van Amerongen et al., 2008). Diverse Fzd receptors have been shown to modulate events
515 that establish neuronal morphology including axonal polarity and growth, axon guidance, dendrite
516 morphogenesis and synaptogenesis (Pascual-Vargas & Salinas, 2021). In particular, Fzd3, 5 and 9
517 have been reported to be essential for axon outgrowth and guidance (Pascual-Vargas & Salinas,
518 2021). In embryonic cortical neurons (E15.5-16.5), we observed that Fzd1, 2, 3, 7, 8 and 9 are
519 expressed at varying levels. Of these Fzds, individual knockdown of Fzd1, 3 or 9 attenuated both
520 basal and sEV-induced neurite outgrowth, whereas Fzd7 was only required for neurite outgrowth
521 mediated by sEVs. This indicates that Fzd1, 3 and 9 act in a non-redundant manner and that Fzd7
522 is specifically required for sEV-mediated effects. Consistently, a non-redundant role for Fzd3 in
523 mediating axon outgrowth and guidance in knockout mouse models has been described (Hua et
524 al., 2013; Hua et al., 2014; Qu et al., 2014). The cell surface and intracellular distribution of Fzds
525 can be modulated by post-translational modifications such as phosphorylation (Pascual-Vargas &
526 Salinas, 2021). Moreover, in neurons, a distinctive spatiotemporal localization of Fzds in the soma,
527 axon and growth cone during different developmental stages has been observed (Sahores et al.,
528 2010; Varela-Nallar et al., 2012; Slater et al., 2013). This differential localization of Fzds in space
529 and time, due at least in part to changes in post-translational modifications, could be critical for
530 axon formation and outgrowth, and thus may explain the non-redundant role of Fzds during this
531 process. Dvls are shared by PCP and canonical Wnt pathways and have been reported to modulate
532 axon outgrowth and guidance (Gao & Chen, 2010; Sharma et al., 2018). For instance, Dvl2 has
533 been reported to specifically function in PCP signaling (Onishi et al., 2013). We observed that
534 cortical neurons express all three Dvls (Dvl1, 2 and 3), but only Dvl2 was required for sEV-
535 induced neurite outgrowth, a process that we have shown requires PCP signaling. Altogether our

536 data indicates a key role for the PCP pathway in regulating neuronal polarization and axon
537 outgrowth that is enhanced by fibroblast-derived sEVs.
538
539 In vertebrates, Wnts are required for the activation of PCP signaling and can modulate neuronal
540 morphology (Butler & Wallingford, 2017; Teo & Salinas, 2021; Koca et al., 2022). Our data shows
541 that neuronal Wnt secretion is required for axon formation as chemical inhibition of porcupine or
542 siRNA-mediated knockdown of Wls, both of which block Wnt secretion, prevented axonogenesis.
543 This observation is consistent with a previous report showing that treatment with the porcupine
544 inhibitor, IWP2, inhibits neuronal polarization in hippocampal neurons (Stanganello et al., 2019).
545 Moreover, we observed that sEV-induced neurite outgrowth was inhibited upon blocking neuronal
546 Wnt secretion. We showed that cortical neurons express Wnt5a, 5b, 7a and 7b, three of which
547 (Wnt5b, 7a and 7b) are required for the growth of the prospective axon and for enhanced axon
548 elongation induced by sEVs. Intracellular association of Wnts with exosomes is critical for Wnt
549 secretion on exosomes (Routledge & Scholpp, 2019; Gross, 2021; Mittermeier & Virshup, 2022).
550 Consistent with this, we showed that neuronal Wnt7b, the most highly expressed Wnt in E15.5
551 cortical neurons, can colocalize with the exogenously applied CD81-positive sEVs within the
552 neurons. This suggests the possibility that sEVs internalized by neurons can engage endogenous
553 Wnts in the context of neurite outgrowth. In a prior study in cancer cells, we showed that exosomes
554 from fibroblasts acquire Wnt11 when internalized by breast cancer cells to activate autocrine Wnt-
555 PCP signaling and promote cell motility and formation of protrusions (Luga et al., 2012). Thus,
556 we speculate that sEVs might similarly activate autocrine Wnt-PCP signaling in neurons to
557 promote axon outgrowth, though precisely how, remains to be explored.
558
559 Although the fibroblasts used in our study were derived from skin, lung and mouse embryos, and
560 thus do not reside in CNS, the current study identifies a potential of fibroblast-derived sEVs,
561 irrespective of the tissue origin, in activating axon outgrowth systems, and thus provides evidence
562 of the therapeutic potential of fibroblast sEVs in treating neuronal injury. At the molecular level,
563 we have shown that sEVs induce axon elongation and a polarized neuronal morphology by
564 engaging Wnt-PCP signaling components. As context-dependent effects of exosomes are not well
565 understood, it will be critical to explore the molecular determinants in exosomes that confer
566 context specificity in varying biological functions.

Acknowledgements

We thank Lisa Qiu, Victoria Leon Guerrero, Bruno Sangiorgi and Nadia Zafar for contributions during the early stages of the project. We thank Dr. Sachdev Sidhu for kindly providing Fzd blocking antibody. This work was funded by grants to L.A. from the CIHR (FDN148455) and to L.A. and J.W. from the Krembil Foundation.

Competing Interests

The authors declare that they have no competing interests.

577 **Materials and Methods**

578 **Mice**

579 Mouse studies were conducted in accordance with the guidelines of the Canadian Council on
580 Animal Care (CCAC) and approved by the University Animal Care Committee, University of
581 Toronto or The Centre for Phenogenomics (TCP), Toronto, Ontario, Canada. Mice were housed
582 in individually ventilated cages with free access to standard animal food and water in a climate-
583 controlled room with a 12 h light/dark cycle. CD1 pregnant females E15-16 were purchased from
584 Charles River.

585

586 Prickle1 (Pk1) conditional knockout mice were generated by introducing Pk1 targeting vector
587 (EUCOMM, HTGR03009_Z_6_E08) into G4 embryonic stem (ES) cells by electroporation. ES
588 cell colonies were selected using Neomycin (Invitrogen, 10131027) and genomic DNA was
589 analyzed by southern blotting to identify homologous recombinants. Chimeric embryos were
590 produced, at the Transgenic Core of the TCP facility, by diploid aggregation of in house generated
591 Pk1 or commercially acquired targeted Pk2 (HEPD0638_2_E01 clone C3) ES cells and CD1
592 embryos. Chimeric mice were crossed with ICRs mice, obtained from TCP, to obtain the F1
593 heterozygotes, that were then crossed with Flp recombinase mice to remove the neomycin
594 selection cassette. For the Pk1 allele, genomic DNA was digested with NdeI and probed with a
595 Pk1 3′ probe, resulting in a 15.7 kb (wild-type allele) and a 10.4 kb (mutant allele) fragment. For
596 the Pk2 allele, genomic DNA was digested with BstEII, ScaI, NsiI, AvrII, or Bsu36 and probed
597 with a Neo probe to produce targeted bands of 15Kb, 18.5Kb, 17.6 Kb, 9.5Kb or 12.7Kb,
598 respectively. Single floxed mice ($Pk1^{fl/fl}$; $Pk2^{+/+}$ and $Pk1^{+/+}$; $Pk2^{fl/fl}$) were crossed with each other
599 to obtain Pk1/2 double floxed mice ($Pk1^{fl/fl}$; $Pk2^{fl/fl}$). To obtain the brain specific conditional
600 knockout, single floxed mice and double floxed mice were crossed with a Nestin-Cre line, acquired
601 from TCP, to obtain Cre+ ($Pk1^{fl/fl}$;$Pk2^{+/+}$;Cre+, $Pk1^{+/+}$;$Pk2^{fl/fl}$;Cre+, $Pk1^{fl/fl}$;$Pk2^{fl/fl}$;Cre+) and Cre-
602 ($Pk1^{fl/fl}$; $Pk2^{+/+}$;Cre-, $Pk1^{+/+}$;$Pk2^{fl/fl}$;Cre-, $Pk1^{fl/fl}$; $Pk2^{fl/fl}$;Cre-) floxed mice that were subsequently
603 crossed with each other to obtain the various genotype combinations. For genotyping, genomic
604 DNA from 2 mm E16.5 tail piece was isolated and then subjected to PCR using primers listed in
605 Table S1. Loss of Pk1/2 expression was confirmed in brain sections from $Pk1^{fl/fl}$; $Pk2^{fl/fl}$;Nestin-
606 Cre+ mice by immunostaining with Pk1/2 antibodies (Table S3), followed by confocal
607 microscopy.

608

609 Heterozygous Vangl2$^{Lp/+}$ (Vangl2^{S464N}) mice (Strong & Hollander, 1949), obtained from Jackson
610 Labs (#000220), were kindly provided by Dr. Helen McNeil (Lunenfeld-Tanenbaum Research
611 Institute, Mount Sinai Hospital, Toronto, Ontario, Canada) and crossed with each other to obtain
612 homozygous mutants (Vangl2$^{Lp/Lp}$). Smurf1/2 heterozygous mice (Smurf1$^{+/-}$; Smurf2$^{+/-}$) were
613 generated previously (Narimatsu et al., 2009), and crossed with each other to generate single
614 knockout (Smurf1$^{-/-}$ or Smurf2$^{-/-}$) embryos.

615

616 **Isolation, culturing and transfection of mouse cortical neurons**

617 Primary cortical neurons were isolated from mouse embryos E15.5-16.5 as previously described
618 (Christova et al., 2023). Briefly, brains were harvested and placed in ice-cold HBSS (Gibco) and
619 cerebral cortices were dissected. Cortices were digested in 0.25 % Trypsin-EDTA (Gibco,
620 25200056) at 37°C followed by trypsin inactivation by adding Dulbecco's Modified Eagle
621 Medium (DMEM) (Gibco, 11995-065) containing 10% FBS (Gibco, 12483-020). After further
622 mechanical dissociation, neurons were seeded at a density of 30000 cells/well for regular
623 experiments or 125,000 cells/well for transfection experiments in 4-well chamber slides (Lab-Tek
624 II, 155382) coated with poly-L-lysine (20 µg/mL, Sigma, P1399) and laminin (2 µg/mL, Corning,
625 354232). Neurons were cultured at 37°C and 5% CO_2 in Neurobasal medium (Gibco, 21103-049)
626 supplemented with 2% B-27 (Gibco, 17504-044), 0.5% N-2 (Gibco, 17502-048), 2 mM
627 GlutaMAX™ (Gibco, 35050-061) and 0.5% penicillin/streptomycin (Gibco, 15140-122).

628

629 For transfections, dissociated neurons were electroporated with cDNA (2 µg) or siRNA (Table S2)
630 using an Amaxa nucleofector (program-005, Lonza) and mouse neuron nucleofector™ kit (VPG-
631 1001, Lonza) according to the manufacturer's instructions. Briefly, neurons (4-5 × 10^6) were
632 electroporated with a mix of 2 µM siGENOME SMARTpool siRNAs (Dharmacon), comprised of
633 a pool of four individual siRNAs except for siWnt7a pool which contained two individual siRNAs
634 (Table S2), and 2 µg of enhanced green fluorescent protein (eGFP) as a transfection reporter.
635 Media was replaced 4 h after seeding. All DNAs were prepared using Endotoxin- Free Maxi-prep
636 kit (Qiagen).

637

638

639 **Mammalian cell culture and transfection**

640 L cells (CRL-2648), Human Dermal fibroblasts (HDFn) (PCS-201-010™), BJ cells (CRL-
641 2522™) and MDA-MB-231 cells were purchased from ATCC, normal Human Lung Fibroblasts
642 (NHLF) were purchased from Lonza (CC-2512) and mouse embryonic fibroblasts (MEFs) were
643 acquired from the TCP facility. MDA-MB-231 cells were cultured in Roswell Park Memorial
644 Institute (RPMI) 1640 medium containing 5% FBS while all other lines were cultured in DMEM
645 containing 10% FBS. Cell lines were routinely tested for mycoplasma contamination using
646 MycoAlert™ Plus reagent (Lonza, LT07-703).

647

648 For siRNA transfections, L cells were (1×10^6) were transfected with 40 nM siGENOME
649 SMARTpool siRNAs (Dharmacon) using Lipofectamine™ RNAiMAX reagent (Invitrogen,
650 13778075) according to manufacturer's protocols. For cDNA transfection of MDA-MB-231 cells,
651 plasmids (2 µg) were delivered using Lipofectamine® 3000 (Invitrogen, L3000-001) according to
652 manufacturer's instructions. The Wnt7b construct was generated using Gateway system (Life
653 Technologies) by transfer from an entry clone into a C-terminal HA-tagged pCMV5-based
654 destination vector.

655

656 **Primary Astrocyte Cultures**

657 Dissociated primary astrocytes were isolated from the cortices of CD1 mouse post-natal (P1-P4)
658 pups as previously published (Schildge et al., 2013). Dissociated cells were cultured in DMEM
659 supplemented with heat inactivated 10% FBS and 1% penicillin/streptomycin in 75 cm^2 flasks
660 (Corning, 430720U) coated with poly-D-lysine (50 µg/mL, Sigma, P7280). Media was changed
661 after 24 h of initial seeding, and every 2 days thereafter. Cultures were grown for 8 days. and then
662 shaken at 120 rpm overnight to remove microglia and less adherent cells. Cells were then washed,
663 trypsinized and these astrocyte enriched cultures were used for subsequent experiments.

664

665 For 3D cultures, astrocytes were seeded in a gel containing type-I rat tail collagen (Ibidi, 50201),
666 prepared according to the manufacturer's protocol. Briefly, 10% minimum essential media (MEM,
667 Gibco, 11430-030), 1% GlutaMAX™ and collagen (2 mg/mL) were mixed on ice and neutralized
668 using 1M NaOH. Subsequently, DMEM containing cells was gently added to the gel mixture
669 resulting in a cell density of 2×10^6 cells/mL of gel mixture. Gel mixture was transferred to either

670 6-well plates (2.5 mL/well) for sEV isolation or in chamber slides (700 μL/well) for
671 immunofluorescence microscopy. The liquid gel mixture was placed at 37°C and 5% CO_2 for 30
672 minutes to solidify and then fresh DMEM containing heat inactivated 10% FBS and 1%
673 penicillin/streptomycin was added.
674
675 **Preparation of Conditioned Media**
676 Fibroblasts (0.5×10^6) were seeded in a 100 mm dish and grown to confluency. Cells were washed
677 with DMEM and incubated with DMEM either without FBS (L cells) or exosome free 10% FBS
678 (for NHLF, HDFn, BJ, MEFs) (Gibco). After 3-4 days, conditioned media (CM) was collected,
679 centrifuged at 300 x g to remove cells and stored at 4 °C. CM from neurons was prepared from
680 primary cortical neurons (4×10^6 cells) seeded in a 100 mm dish and cultured in a serum free
681 complete medium. On day 4, 25% of freshly made complete medium supplemented with 5 μM
682 cytosine β-d-arabinofuranoside (Sigma, C1768) was added and CM was collected on day 8. For
683 2D astrocytes, enriched primary astrocytes cells were seeded in p75 flasks and cultured in DMEM
684 supplemented with heat inactivated exosome free 10% FBS. Cultures were grown to confluency,
685 and the CM was collected after 6 days. For 3D astrocytes cultures in collagen gel, enriched primary
686 astrocytes were seeded in 6 well plate and CM was collected after 6 days. Small EVs from
687 fibroblast-CM were purified within 1 week, whereas sEVs from neurons and astrocytes were
688 isolated on the same day.
689
690 **Isolation of small extracellular vesicles (sEVs)**
691 Conditioned media (CM) (50 mL) was collected from fibroblasts, neurons or astrocytes and
692 centrifuged at 300 x g for 5 min and at 2000 x g for 20 min to remove cells and large debris,
693 respectively. Supernatants were then centrifuged at 10,000 x g for 30 min to remove apoptotic
694 bodies and large vesicles. The resulting supernatants were filtered through a 0.2 μm filter (Thermo
695 Fisher Scientific, 568-0020) and ultracentrifuged at 100,000 x g (Type 70 Ti rotor, Beckman
696 Coulter) for 2 h using 25 × 89 mm polycarbonate tubes (Beckman Coulter, 355618). Pellets were
697 resuspended in 500 μL of sterile phosphate-buffered saline (PBS) and diluted with 7.5 mL of PBS.
698 Diluted pellets were ultracentrifuged at 100,000 x g (Type 70.1 Ti rotor, Beckman Coulter) for 2
699 h using 16 × 76 mm polycarbonate tubes (Beckman Coulter, 355603). The resulting pellets were
700 resuspended in 250 μL of sterile PBS, aliquoted and stored at -80°C.

701

702 **Purification of sEVs using iodixanol density gradient**

703 A discontinuous iodixanol gradient, prepared by diluting 60% iodixanol (Optiprep™, Sigma,
704 D1556) with 0.25 M sucrose / 10 mM Tris, pH 7.4, was used to further purify the sEV pellets
705 (100,000 x g). The sEV pellet, resuspended in 500 μL of PBS, was overlaid on top of the
706 discontinuous gradient (40%, 20%, 10% and 5%; 3 mL each, but 2.5 mL for 5%) and
707 ultracentrifuged at 100,000 x g (SW 40 Ti or SW41 Ti rotor, Beckman Coulter) for 16 h using
708 ultra-clear tubes (Beckman Coulter, 344060 or 344059). Twelve fractions of 1 mL each were
709 collected manually from the top. Fractions were washed by diluting with 7 mL of PBS and
710 ultracentrifuged at 100,000 x g (Type 70.1 Ti rotor, Beckman Coulter) for 2 h. The resulting pellets
711 were resuspended in 150 μL of sterile PBS and stored at -80°C.

712

713 **Purification of sEVs by size exclusion chromatography**

714 The sEV pellets (100,000 x g) were purified using qEV original size exclusion column with a pore
715 size of 70 nm (Izon science, 1001683) according to manufacturer's protocol with minor
716 modifications. Briefly, the column was equilibrated with 30 mL of PBS and exosome pellet,
717 resuspended in 500 μL of PBS, was overlaid on qEV column followed by elution with PBS.
718 Fractions of 500 μL were collected and analyzed for particle and protein concentration using NTA
719 and Bradford assay, respectively.

720

721 **Purification of sEVs by Exo-spin™ precipitation**

722 The sEVs from 3D-astrocytes were purified using Exo-spin™ purification kit (Cell Guidance
723 Systems) according to manufacturer's instructions. Briefly, CM was precleared by sequential
724 centrifugations at 300 x g, 2000 x g and 10,000 x g. Supernatants were mixed with the precipitation
725 buffer and incubated overnight at 4°C. Samples were centrifuged at 10,000 x g for 30 min and
726 pellets were re-suspended in 200 μL of PBS. Samples were further purified using provided size
727 exclusion columns and exosomes were eluted in 200 μL of PBS.

728

729

730

731

732 **Proteinase K and detergent treatment of sEVs**

733 sEVs were incubated with a final concentration of 100 μg/mL Proteinase K or 1% Triton X-100
734 at 37°C for 1 hour with gentle vortexing every 15 min. After treatment, sEVs were washed in 7
735 mL of PBS, ultracentrifuged for 2 h and the resulting pellet was resuspended in 120 μL of PBS.

736

737 **Nanoparticle Tracking Analysis**

738 The number of particles were measured using ZetaView® PMX 110 device (Particle Metrix
739 GmbH, Germany). The measurements were taken at all 11 different positions with camera
740 sensitivity set to 90 and shutter speed at 45 using the ZetaView software (version 8.03.08). The
741 video quality was set to medium, and the data was analyzed using the ZetaView analysis software
742 (version 8.02.31) with the following post-acquisition parameters: minimum size 10, maximum size
743 1000, and minimum brightness 20.

744

745 **Small EV internalization assay**

746 For sEV internalization assays, 50 mL of media was collected from L cells stably transfected with
747 either CD81-EYFP or CD81-pLVX as a control (Luga et al., 2012). CM was centrifuged at 300 x
748 g for 5 min and at 2000 x g for 20 min to remove cells and large debris, respectively. Supernatants
749 were concentrated 10-fold using a 10 kDa MWCO filter (Amicon® Ultra-15, UFC901008).
750 Neurons were seeded in 8 well Ibidi chambers and treated with 10X CM for 29 h or 30 min, prior
751 to fixation, immunostaining and imaging using confocal microscopy.

752

753 **Neurite outgrowth assay in a microfluidic chamber**

754 Two compartment microfluidic chambers containing a 150 μm microgroove were purchased from
755 Xona Microfluidics (XC150). Chambers were prepared for seeding neurons according to
756 manufacturer's instructions with a few modifications. Briefly, chambers were treated with a pre-
757 coat solution and subsequently coated with poly-L-lysine (20 μg/mL) and laminin (2 μg/mL).
758 Cortical neurons (50,000 cells) were seeded in one well in an initial volume of 20 μL and allowed
759 to adhere for 5 min at 37°C and 5% CO_2. Complete Neurobasal medium was added to all the wells
760 and neurons cultured for 5 days until axons crossed the microgroove and emerged in the distal
761 chamber. The sEVs (5 μg/mL) were added either to the somal side or axonal sides on day 5 for 24
762 h prior to fixation and immunostaining.

763

764 **RT and qPCR**

765 For neurons and astrocytes, total RNA was extracted using the Norgen Single-Cell RNA
766 Purification Kit (Norgen, 51800). For other cells, total RNA was extracted using PureLink RNA
767 Mini Kit (Life Technologies, 12183025). Complementary DNA was synthesized using 35 to 200
768 ng of purified RNA using oligo-dT primers and M-MLV Reverse Transcriptase (Invitrogen,
769 28025-013). Real-time qPCR was performed using SYBR^{TM} Green PCR Master Mix (Applied
770 Biosciences, 4309155) on the QuantStudio 6 Flex System (Applied Biosciences). Relative gene
771 expression was quantified using the ΔΔCt method and normalized to glyceraldehyde-3-phosphate
772 dehydrogenase (Gapdh). Primers used are listed in the Supplementary Table S4.

773

774 **Immunofluorescence microscopy and immunoblotting**

775 For immunocytochemistry, neurons and astrocytes were fixed in 4% paraformaldehyde as
776 previously described (Christova et al., 2023). Briefly, cells were permeabilized with 0.2%
777 Triton/PBS, washed with PBS, and blocked at room temperature for 1 h with 3% Bovine Serum
778 Albumin (BSA)/PBS. Cells were incubated with primary antibodies for 2 h at room temperature
779 or overnight at 4°C, washed 3 times with PBS, and incubated with secondary antibodies for 2 h at
780 room temperature. Cells were washed with PBS and stored in PBS or in Ibidi mounting medium
781 prior to imaging. For immunohistochemistry of mouse embryos at E15.5, embryos were fixed in
782 4% paraformaldehyde in PBS at 4°C overnight. After washing with 0.1% Tween 20 in PBS (PBST)
783 3 times for 5 min, the samples were cryoprotected by immersing in 15% sucrose in PBS at 4°C
784 overnight, then 30% sucrose in PBS at 4°C overnight. Samples were embedded in optimum cutting
785 temperature (OCT) compound and cyrosections of 16 μm were prepared with a cryostat (Leica
786 Biosytems, CM3050 S), which were then stained with antibodies listed in Table S3. For
787 epifluorescence microscopy, images were acquired using the 40X Plan-NEOFLUAR objective of
788 Zeiss Axiovert 200 M epifluorescence microscope. For confocal microscopy, images were
789 acquired using Zeiss AXIO Observer Z1 microscope equipped with Zen Blue software, a spinning
790 disc confocal scanner (CSU-X1, Yokogawa) and a CCD camera (Axiocam 506 mono) with
791 following objectives: Plan-Apochromat 20x/0.8 M27 air, Plan-Apochromat 40x/1.4 Oil DIC and
792 Plan-Apochromat 63x/1.4 Oil DIC M27. Some confocal images were acquired using Nikon
793 ECLIPSE Ti2 inverted microscope equipped with LUA-S laser unit and NIS-Elements software

794 (from Nikon) with following objectives: Nikon-N Apo-LWD 40X/1.15 WI and Nikon-N Apo-
795 LWD 20X/0.95 WI. All images were acquired in a random fashion.
796
797 For immunoblotting, cells were lysed in lysis buffer (50 mM Tris-HCl, 150 mM NaCl, 1 mM
798 EDTA, 0.5% Triton X-100, 1 mM DTT containing protease and phosphatase inhibitors) (Bao et
799 al., 2012). Protein concentration was determined using Bradford reagent (BIORAD). Proteins from
800 cell lysates (1-20 μg) and exosomes (1-10 μg) were separated on an SDS-PAGE gel and analyzed
801 by immunoblotting as described previously (Heidary Arash et al., 2014).
802
803 **Electron microscopy**
804 Exosomes were visualized using Talos L120C transmission electron microscope (TEM) (Thermo
805 Scientific) in the Microscopy Imaging Laboratory, University of Toronto, Canada. The sEV
806 samples were frozen on TEM grids (Quantifoil R2,2 300 mesh, EMS) that were charged for 30
807 seconds with a Pelco EasiGlow glow discharge cleaning system (Ted Pella). Samples (4 μL) were
808 deposited onto the grid and the grid was blotted and plunge frozen using a Vitrobot IV (FEI).
809 Images were taken using 120kV at magnifications 28000x and 57000x, corresponding to a pixel
810 size of 510 and 249 pm respectively. Images were collected at a defocus of -4 to -1.5 microns using
811 the TEM Image and Analysis (TIA) software.
812
813 **Quantification**
814 For Tuj1 stained neurons, the length of all neurites (including the longest neurite, a prospective
815 axon, and dendrites, all other neurites excluding the longest neurite) were quantified using
816 Volocity software (Quorum Technologies Inc, Canada). In MAP2 and Tau-1 experiments, neurons
817 were classified into two groups: only MAP2-positive minor neurites or minor neurites and a single
818 Tau-1-positive axon displaying medial-to-distal localization of the Tau-1.
819
820 For Vangl2 localization, the intensity of Vangl2 in soma, proximal axon and distal axon was
821 quantified using Nikon NIS-Elements software (Version 5.41.00). For sEVs and Wnt7b co-
822 localization, neurons were identified using Tuj1 as a reference channel and the Pearson's
823 colocalization coefficient for GFP (sEVs) and Wnt7b was determined using Nikon NIS-Elements
824 software (Version 5.41.00).

825

826 **Statistical Analyses**

827 The data for the axon length and longest neurite length is plotted as a violin plot from 90-120
828 neurons per condition in 3 independent experiments. The data was analyzed statistically using an
829 unpaired t-test for comparing two groups or one-way ANOVA with Dunnetts post-test for multiple
830 comparisons to a single control group, or two-way ANOVA with Tukey's post-test for multiple
831 comparisons to control and between samples, as indicated in the figure legends. All statistics were
832 done in GraphPad PRISM 9 (GraphPad software Inc. La Jolla, CA). Statistical significance:
833 *$p<0.05$, **$p<0.01$, ***$p<0.001$.

834

835 **References**
836

837 Arimura N, Kaibuchi K (2007) Neuronal polarity: from extracellular signals to intracellular
838 mechanisms. *Nat Rev Neurosci* 8: 194-205.

839 Bahram Sangani N, Gomes AR, Curfs LMG, Reutelingsperger CP (2021) The role of
840 Extracellular Vesicles during CNS development. *Prog Neurobiol* 205: 102124.

841 Banziger C, Soldini D, Schutt C, Zipperlen P, Hausmann G, Basler K (2006) Wntless, a
842 conserved membrane protein dedicated to the secretion of Wnt proteins from signaling cells. *Cell*
843 125: 509-522.

844 Bao R, Christova T, Song S, Angers S, Yan X, Attisano L (2012) Inhibition of tankyrases
845 induces Axin stabilization and blocks Wnt signalling in breast cancer cells. *PLoS One* 7: e48670.

846 Belotti E, Puvirajesinghe TM, Audebert S, Baudelet E, Camoin L, Pierres M, Lasvaux L,
847 Ferracci G, Montcouquiol M, Borg JP (2012) Molecular characterisation of endogenous
848 Vangl2/Vangl1 heteromeric protein complexes. *PLoS One* 7: e46213.

849 Bonansco C, Cerpa W, Inestrosa NC (2022) How Are Synapses Born? A Functional and
850 Molecular View of the Role of the Wnt Signaling Pathway. *Int J Mol Sci* 24: 708.

851 Bonsergent E, Grisard E, Buchrieser J, Schwartz O, Thery C, Lavieu G (2021) Quantitative
852 characterization of extracellular vesicle uptake and content delivery within mammalian cells. *Nat*
853 *Commun* 12: 1864.

854 Bradke F (2022) Mechanisms of Axon Growth and Regeneration: Moving between Development
855 and Disease. *J Neurosci* 42: 8393-8405.

856 Butler MT, Wallingford JB (2017) Planar cell polarity in development and disease. *Nat Rev Mol*
857 *Cell Biol* 18: 375-388.

858 Buzas EI (2023) The roles of extracellular vesicles in the immune system. *Nat Rev Immunol* 23:
859 236-250.

860 Chen B, Dodge ME, Tang W, Lu J, Ma Z, Fan CW, Wei S, Hao W, Kilgore J, Williams NS *et al*
861 (2009) Small molecule-mediated disruption of Wnt-dependent signaling in tissue regeneration
862 and cancer. *Nat Chem Biol* 5: 100-107.

863 Cheng PL, Lu H, Shelly M, Gao H, Poo MM (2011) Phosphorylation of E3 ligase Smurf1
864 switches its substrate preference in support of axon development. *Neuron* 69: 231-243.

865 Chivet M, Javalet C, Hemming F, Pernet-Gallay K, Laulagnier K, Fraboulet S, Sadoul R (2013)
866 Exosomes as a novel way of interneuronal communication. *Biochem Soc Trans* 41: 241-244.

867 Christova T, Ho SK, Liu Y, Gill M, Attisano L (2023) LTK and ALK promote neuronal polarity
868 and cortical migration by inhibiting IGF1R activity. *EMBO Rep* 24: e56937.

869 Clarke LE, Barres BA (2013) Emerging roles of astrocytes in neural circuit development. *Nat*
870 *Rev Neurosci* 14: 311-321.

871 Clarke LE, Liddelow SA, Chakraborty C, Munch AE, Heiman M, Barres BA (2018) Normal
872 aging induces A1-like astrocyte reactivity. *Proc Natl Acad Sci U S A* 115: E1896-E1905.

873 Colombo M, Raposo G, Thery C (2014) Biogenesis, secretion, and intercellular interactions of
874 exosomes and other extracellular vesicles. *Annu Rev Cell Dev Biol* 30: 255-289.

875 Cvjetkovic A, Jang SC, Konecna B, Hoog JL, Sihlbom C, Lasser C, Lotvall J (2016) Detailed
876 Analysis of Protein Topology of Extracellular Vesicles-Evidence of Unconventional Membrane
877 Protein Orientation. *Sci Rep* 6: 36338.

878 Dai J, Su Y, Zhong S, Cong L, Liu B, Yang J, Tao Y, He Z, Chen C, Jiang Y (2020) Exosomes:
879 key players in cancer and potential therapeutic strategy. *Signal Transduct Target Ther* 5: 145.

880 Davey CF, Moens CB (2017) Planar cell polarity in moving cells: think globally, act locally.
881 *Development* 144: 187-200.

882 Devenport D (2016) Tissue morphodynamics: Translating planar polarity cues into polarized cell
883 behaviors. *Semin Cell Dev Biol* 55: 99-110.

884 Dorrego-Rivas A, Ezan J, Moreau MM, Poirault-Chassac S, Aubailly N, De Neve J, Blanchard
885 C, Castets F, Freal A, Battefeld A *et al* (2022) The core PCP protein Prickle2 regulates axon
886 number and AIS maturation by binding to AnkG and modulating microtubule bundling. *Sci Adv*
887 8: eabo6333.

888 Dos-Santos Carvalho S, Moreau MM, Hien YE, Garcia M, Aubailly N, Henderson DJ, Studer V,
889 Sans N, Thoumine O, Montcouquiol M (2020) Vangl2 acts at the interface between actin and N-
890 cadherin to modulate mammalian neuronal outgrowth. *Elife* 9: e51822.

891 Dotti CG, Sullivan CA, Banker GA (1988) The establishment of polarity by hippocampal
892 neurons in culture. *J Neurosci* 8: 1454-1468.

893 Dreesmann L, Mittnacht U, Lietz M, Schlosshauer B (2009) Nerve fibroblast impact on Schwann
894 cell behavior. *Eur J Cell Biol* 88: 285-300.

895 Dreyer CA, VanderVorst K, Carraway KL, 3rd (2022) Vangl as a Master Scaffold for
896 Wnt/Planar Cell Polarity Signaling in Development and Disease. *Front Cell Dev Biol* 10:
897 887100.

898 East E, Golding JP, Phillips JB (2009) A versatile 3D culture model facilitates monitoring of
899 astrocytes undergoing reactive gliosis. *J Tissue Eng Regen Med* 3: 634-646.

900 Escartin C, Galea E, Lakatos A, O'Callaghan JP, Petzold GC, Serrano-Pozo A, Steinhauser C,
901 Volterra A, Carmignoto G, Agarwal A *et al* (2021) Reactive astrocyte nomenclature, definitions,
902 and future directions. *Nat Neurosci* 24: 312-325.

903 Fan Y, Chen Z, Zhang M (2022) Role of exosomes in the pathogenesis, diagnosis, and treatment
904 of central nervous system diseases. *J Transl Med* 20: 291.

905 Gao C, Chen YG (2010) Dishevelled: The hub of Wnt signaling. *Cell Signal* 22: 717-727.

906 Gassama Y, Favereaux A (2021) Emerging Roles of Extracellular Vesicles in the Central
907 Nervous System: Physiology, Pathology, and Therapeutic Perspectives. *Front Cell Neurosci* 15:
908 626043.

909 Goodrich LV (2008) The plane facts of PCP in the CNS. *Neuron* 60: 9-16.

910 Goodrich LV, Strutt D (2011) Principles of planar polarity in animal development. *Development*
911 138: 1877-1892.

912 Gross JC (2021) Extracellular WNTs: Trafficking, Exosomes, and Ligand-Receptor Interaction.
913 *Handb Exp Pharmacol* 269: 29-43.

914 Hakanen J, Ruiz-Reig N, Tissir F (2019) Linking Cell Polarity to Cortical Development and
915 Malformations. *Front Cell Neurosci* 13: 244.

916 Heidary Arash E, Song KM, Song S, Shiban A, Attisano L (2014) Arhgef7 promotes activation
917 of the Hippo pathway core kinase Lats. *EMBO J* 33: 2997-3011.

918 Hua ZL, Jeon S, Caterina MJ, Nathans J (2014) Frizzled3 is required for the development of
919 multiple axon tracts in the mouse central nervous system. *Proc Natl Acad Sci U S A* 111: E3005-
920 3014.

921 Hua ZL, Smallwood PM, Nathans J (2013) Frizzled3 controls axonal development in distinct
922 populations of cranial and spinal motor neurons. *Elife* 2: e01482.

923 Jones C, Chen P (2007) Planar cell polarity signaling in vertebrates. *Bioessays* 29: 120-132.

924 Kalluri R, LeBleu VS (2020) The biology, function, and biomedical applications of exosomes.
925 *Science* 367.

926 Kannan M, Lee SJ, Schwedhelm-Domeyer N, Stegmuller J (2012) The E3 ligase Cdh1-anaphase
927 promoting complex operates upstream of the E3 ligase Smurf1 in the control of axon growth.
928 *Development* 139: 3600-3612.

929 Kibar Z, Vogan KJ, Groulx N, Justice MJ, Underhill DA, Gros P (2001) Ltap, a mammalian
930 homolog of Drosophila Strabismus/Van Gogh, is altered in the mouse neural tube mutant Loop-
931 tail. *Nat Genet* 28: 251-255.

932 Koca Y, Collu GM, Mlodzik M (2022) Wnt-frizzled planar cell polarity signaling in the
933 regulation of cell motility. *Curr Top Dev Biol* 150: 255-297.

934 Lee HG, Wheeler MA, Quintana FJ (2022) Function and therapeutic value of astrocytes in
935 neurological diseases. *Nat Rev Drug Discov* 21: 339-358.

936 Liddelow SA, Barres BA (2017) Reactive Astrocytes: Production, Function, and Therapeutic
937 Potential. *Immunity* 46: 957-967.

938 Liu J, Pan S, Hsieh MH, Ng N, Sun F, Wang T, Kasibhatla S, Schuller AG, Li AG, Cheng D *et*
939 *al* (2013) Targeting Wnt-driven cancer through the inhibition of Porcupine by LGK974. *Proc*
940 *Natl Acad Sci U S A* 110: 20224-20229.

941 Lopez-Verrilli MA, Caviedes A, Cabrera A, Sandoval S, Wyneken U, Khoury M (2016)
942 Mesenchymal stem cell-derived exosomes from different sources selectively promote neuritic
943 outgrowth. *Neuroscience* 320: 129-139.

944 Lopez-Verrilli MA, Picou F, Court FA (2013) Schwann cell-derived exosomes enhance axonal
945 regeneration in the peripheral nervous system. *Glia* 61: 1795-1806.

946 Luga V, Zhang L, Viloria-Petit AM, Ogunjimi AA, Inanlou MR, Chiu E, Buchanan M, Hosein
947 AN, Basik M, Wrana JL (2012) Exosomes mediate stromal mobilization of autocrine Wnt-PCP
948 signaling in breast cancer cell migration. *Cell* 151: 1542-1556.

949 MacDonald BT, He X (2012) Frizzled and LRP5/6 receptors for Wnt/beta-catenin signaling.
950 *Cold Spring Harb Perspect Biol* 4: a007880.

951 Merte J, Jensen D, Wright K, Sarsfield S, Wang Y, Schekman R, Ginty DD (2010) Sec24b
952 selectively sorts Vangl2 to regulate planar cell polarity during neural tube closure. *Nat Cell Biol*
953 12: 41-46.

954 Mikels AJ, Nusse R (2006) Wnts as ligands: processing, secretion and reception. *Oncogene* 25:
955 7461-7468.

956 Mittermeier L, Virshup DM (2022) An itch for things remote: The journey of Wnts. *Curr Top*
957 *Dev Biol* 150: 91-128.

958 Mlodzik M (2016) The Dishevelled Protein Family: Still Rather a Mystery After Over 20 Years
959 of Molecular Studies. *Curr Top Dev Biol* 117: 75-91.

960 Montcouquiol M, Kelley MW (2020) Development and Patterning of the Cochlea: From
961 Convergent Extension to Planar Polarity. *Cold Spring Harb Perspect Med* 10: a033266.

962 Murdoch JN, Doudney K, Paternotte C, Copp AJ, Stanier P (2001) Severe neural tube defects in
963 the loop-tail mouse result from mutation of Lpp1, a novel gene involved in floor plate
964 specification. *Hum Mol Genet* 10: 2593-2601.

965 Namba T, Funahashi Y, Nakamuta S, Xu C, Takano T, Kaibuchi K (2015) Extracellular and
966 Intracellular Signaling for Neuronal Polarity. *Physiol Rev* 95: 995-1024.

967 Narimatsu M, Bose R, Pye M, Zhang L, Miller B, Ching P, Sakuma R, Luga V, Roncari L,
968 Attisano L *et al* (2009) Regulation of planar cell polarity by Smurf ubiquitin ligases. *Cell* 137:
969 295-307.

970 Niehrs C (2012) The complex world of WNT receptor signalling. *Nat Rev Mol Cell Biol* 13: 767-
971 779.

972 Nusse R, Clevers H (2017) Wnt/beta-Catenin Signaling, Disease, and Emerging Therapeutic
973 Modalities. *Cell* 169: 985-999.

974 Onishi K, Shafer B, Lo C, Tissir F, Goffinet AM, Zou Y (2013) Antagonistic functions of
975 Dishevelleds regulate Frizzled3 endocytosis via filopodia tips in Wnt-mediated growth cone
976 guidance. *J Neurosci* 33: 19071-19085.

977 Parrinello S, Napoli I, Ribeiro S, Wingfield Digby P, Fedorova M, Parkinson DB, Doddrell RD,
978 Nakayama M, Adams RH, Lloyd AC (2010) EphB signaling directs peripheral nerve
979 regeneration through Sox2-dependent Schwann cell sorting. *Cell* 143: 145-155.

980 Pascual-Vargas P, Salinas PC (2021) A Role for Frizzled and Their Post-Translational
981 Modifications in the Mammalian Central Nervous System. *Front Cell Dev Biol* 9: 692888.

982 Pavlovic Z, Adams JJ, Blazer LL, Gakhal AK, Jarvik N, Steinhart Z, Robitaille M, Mascall K,
983 Pan J, Angers S *et al* (2018) A synthetic anti-Frizzled antibody engineered for broadened
984 specificity exhibits enhanced anti-tumor properties. *MAbs* 10: 1157-1167.

985 Pegtel DM, Gould SJ (2019) Exosomes. *Annu Rev Biochem* 88: 487-514.

986 Pekny M, Pekna M (2014) Astrocyte reactivity and reactive astrogliosis: costs and benefits.
987 *Physiol Rev* 94: 1077-1098.

988 Qu Y, Huang Y, Feng J, Alvarez-Bolado G, Grove EA, Yang Y, Tissir F, Zhou L, Goffinet AM
989 (2014) Genetic evidence that Celsr3 and Celsr2, together with Fzd3, regulate forebrain wiring in
990 a Vangl-independent manner. *Proc Natl Acad Sci U S A* 111: E2996-3004.

991 Radaszkiewicz KA, Sulcova M, Kohoutkova E, Harnos J (2023) The role of prickle proteins in
992 vertebrate development and pathology. *Mol Cell Biochem*.

993 Rim EY, Clevers H, Nusse R (2022) The Wnt Pathway: From Signaling Mechanisms to
994 Synthetic Modulators. *Annu Rev Biochem* 91: 571-598.

995 Routledge D, Scholpp S (2019) Mechanisms of intercellular Wnt transport. *Development* 146:
996 dev176073.

997 Sahai E, Garcia-Medina R, Pouyssegur J, Vial E (2007) Smurf1 regulates tumor cell plasticity
998 and motility through degradation of RhoA leading to localized inhibition of contractility. *J Cell*
999 *Biol* 176: 35-42.

1000 Sahores M, Gibb A, Salinas PC (2010) Frizzled-5, a receptor for the synaptic organizer Wnt7a,
1001 regulates activity-mediated synaptogenesis. *Development* 137: 2215-2225.

1002 Salinas PC (2012) Wnt signaling in the vertebrate central nervous system: from axon guidance to
1003 synaptic function. *Cold Spring Harb Perspect Biol* 4: a008003.

1004 Schelski M, Bradke F (2017) Neuronal polarization: From spatiotemporal signaling to
1005 cytoskeletal dynamics. *Mol Cell Neurosci* 84: 11-28.

1006 Schildge S, Bohrer C, Beck K, Schachtrup C (2013) Isolation and culture of mouse cortical
1007 astrocytes. *J Vis Exp*: 50079.

1008 Shafer B, Onishi K, Lo C, Colakoglu G, Zou Y (2011) Vangl2 promotes Wnt/planar cell
1009 polarity-like signaling by antagonizing Dvl1-mediated feedback inhibition in growth cone
1010 guidance. *Dev Cell* 20: 177-191.

1011 Sharma M, Castro-Piedras I, Simmons GE, Jr., Pruitt K (2018) Dishevelled: A masterful
1012 conductor of complex Wnt signals. *Cell Signal* 47: 52-64.

1013 Slater PG, Ramirez VT, Gonzalez-Billault C, Varela-Nallar L, Inestrosa NC (2013) Frizzled-5
1014 receptor is involved in neuronal polarity and morphogenesis of hippocampal neurons. *PLoS One*
1015 8: e78892.

1016 Stanganello E, Zahavi EE, Burute M, Smits J, Jordens I, Maurice MM, Kapitein LC, Hoogenraad
1017 CC (2019) Wnt Signaling Directs Neuronal Polarity and Axonal Growth. *iScience* 13: 318-327.

1018 Steinhart Z, Angers S (2018) Wnt signaling in development and tissue homeostasis.
1019 *Development* 145: dev146589.

1020 Strong LC, Hollander WF (1949) HEREDITARY LOOP-TAIL IN THE HOUSE MOUSE:
1021 Accompanied by Imperforate Vagina and with Lethal Craniorachischisis When Homozygous. *J*
1022 *Hered* 40: 329-334.

1023 Takada R, Satomi Y, Kurata T, Ueno N, Norioka S, Kondoh H, Takao T, Takada S (2006)
1024 Monounsaturated fatty acid modification of Wnt protein: its role in Wnt secretion. *Dev Cell* 11:
1025 791-801.

1026 Takano T, Funahashi Y, Kaibuchi K (2019) Neuronal Polarity: Positive and Negative Feedback
1027 Signals. *Front Cell Dev Biol* 7: 69.

1028 Tao H, Manak JR, Sowers L, Mei X, Kiyonari H, Abe T, Dahdaleh NS, Yang T, Wu S, Chen S
1029 *et al* (2011) Mutations in prickle orthologs cause seizures in flies, mice, and humans. *Am J Hum*
1030 *Genet* 88: 138-149.

1031 Tao H, Suzuki M, Kiyonari H, Abe T, Sasaoka T, Ueno N (2009) Mouse prickle1, the homolog
1032 of a PCP gene, is essential for epiblast apical-basal polarity. *Proc Natl Acad Sci U S A* 106:
1033 14426-14431.

1034 Tao Y, Mis M, Blazer L, Ustav MJ, Steinhart Z, Chidiac R, Kubarakos E, O'Brien S, Wang X,
1035 Jarvik N *et al* (2019) Tailored tetravalent antibodies potently and specifically activate
1036 Wnt/Frizzled pathways in cells, organoids and mice. *Elife* 8: e46134.

1037 Tassew NG, Charish J, Shabanzadeh AP, Luga V, Harada H, Farhani N, D'Onofrio P, Choi B,
1038 Ellabban A, Nickerson PEB *et al* (2017) Exosomes Mediate Mobilization of Autocrine Wnt10b
1039 to Promote Axonal Regeneration in the Injured CNS. *Cell Rep* 20: 99-111.

1040 Taylor AM, Blurton-Jones M, Rhee SW, Cribbs DH, Cotman CW, Jeon NL (2005) A
1041 microfluidic culture platform for CNS axonal injury, regeneration and transport. *Nat Methods* 2:
1042 599-605.

1043 Teo S, Salinas PC (2021) Wnt-Frizzled Signaling Regulates Activity-Mediated Synapse
1044 Formation. *Front Mol Neurosci* 14: 683035.

1045 Thery C, Witwer KW, Aikawa E, Alcaraz MJ, Anderson JD, Andriantsitohaina R, Antoniou A,
1046 Arab T, Archer F, Atkin-Smith GK *et al* (2018) Minimal information for studies of extracellular
1047 vesicles 2018 (MISEV2018): a position statement of the International Society for Extracellular
1048 Vesicles and update of the MISEV2014 guidelines. *J Extracell Vesicles* 7: 1535750.

1049 Torban E, Wang HJ, Patenaude AM, Riccomagno M, Daniels E, Epstein D, Gros P (2007)
1050 Tissue, cellular and sub-cellular localization of the Vangl2 protein during embryonic
1051 development: effect of the Lp mutation. *Gene Expr Patterns* 7: 346-354.

1052 van Amerongen R, Mikels A, Nusse R (2008) Alternative wnt signaling is initiated by distinct
1053 receptors. *Sci Signal* 1: re9.

1054 van Neerven SG, Pannaye P, Bozkurt A, Van Nieuwenhoven F, Joosten E, Hermans E, Taccola
1055 G, Deumens R (2013) Schwann cell migration and neurite outgrowth are influenced by media
1056 conditioned by epineurial fibroblasts. *Neuroscience* 252: 144-153.

1057 van Niel G, Carter DRF, Clayton A, Lambert DW, Raposo G, Vader P (2022) Challenges and
1058 directions in studying cell-cell communication by extracellular vesicles. *Nat Rev Mol Cell Biol*
1059 23: 369-382.

1060 Varela-Nallar L, Ramirez VT, Gonzalez-Billault C, Inestrosa NC (2012) Frizzled receptors in
1061 neurons: from growth cones to the synapse. *Cytoskeleton (Hoboken)* 69: 528-534.

1062 Vohra BP, Fu M, Heuckeroth RO (2007) Protein kinase Czeta and glycogen synthase kinase-
1063 3beta control neuronal polarity in developing rodent enteric neurons, whereas SMAD specific E3
1064 ubiquitin protein ligase 1 promotes neurite growth but does not influence polarity. *J Neurosci* 27:
1065 9458-9468.

1066 Wallingford JB (2012) Planar cell polarity and the developmental control of cell behavior in
1067 vertebrate embryos. *Annu Rev Cell Dev Biol* 28: 627-653.

1068 Wang HR, Zhang Y, Ozdamar B, Ogunjimi AA, Alexandrova E, Thomsen GH, Wrana JL (2003)
1069 Regulation of cell polarity and protrusion formation by targeting RhoA for degradation. *Science*
1070 302: 1775-1779.

1071 Wang M, Marco P, Capra V, Kibar Z (2019) Update on the Role of the Non-Canonical
1072 Wnt/Planar Cell Polarity Pathway in Neural Tube Defects. *Cells* 8: 1198.

1073 Wang Y, Chang H, Rattner A, Nathans J (2016) Frizzled Receptors in Development and Disease.
1074 *Curr Top Dev Biol* 117: 113-139.

1075 Webber J, Clayton A (2013) How pure are your vesicles? *J Extracell Vesicles* 2: 19861.

1076 Welsh JA, Goberdhan DCI, O'Driscoll L, Buzas EI, Blenkiron C, Bussolati B, Cai H, Di Vizio
1077 D, Driedonks TAP, Erdbrugger U *et al* (2024) Minimal information for studies of extracellular
1078 vesicles (MISEV2023): From basic to advanced approaches. *J Extracell Vesicles* 13: e12404.

1079 Willert K, Nusse R (2012) Wnt proteins. *Cold Spring Harb Perspect Biol* 4: a007864.

1080 Xin H, Li Y, Buller B, Katakowski M, Zhang Y, Wang X, Shang X, Zhang ZG, Chopp M (2012)
1081 Exosome-mediated transfer of miR-133b from multipotent mesenchymal stromal cells to neural
1082 cells contributes to neurite outgrowth. *Stem Cells* 30: 1556-1564.

1083 Yang Y, Mlodzik M (2015) Wnt-Frizzled/planar cell polarity signaling: cellular orientation by
1084 facing the wind (Wnt). *Annu Rev Cell Dev Biol* 31: 623-646.

1085 Yates AG, Pink RC, Erdbrugger U, Siljander PR, Dellar ER, Pantazi P, Akbar N, Cooke WR,
1086 Vatish M, Dias-Neto E *et al* (2022) In sickness and in health: The functional role of extracellular
1087 vesicles in physiology and pathology in vivo: Part II: Pathology: Part II: Pathology. *J Extracell*
1088 *Vesicles* 11: e12190.

1089 You Y, Borgmann K, Edara VV, Stacy S, Ghorpade A, Ikezu T (2020) Activated human
1090 astrocyte-derived extracellular vesicles modulate neuronal uptake, differentiation and firing. *J*
1091 *Extracell Vesicles* 9: 1706801.

1092 Zhang Y, Chopp M, Liu XS, Katakowski M, Wang X, Tian X, Wu D, Zhang ZG (2017)
1093 Exosomes Derived from Mesenchymal Stromal Cells Promote Axonal Growth of Cortical
1094 Neurons. *Mol Neurobiol* 54: 2659-2673.

1095 Zhang Y, Liu Y, Liu H, Tang WH (2019) Exosomes: biogenesis, biologic function and clinical
1096 potential. *Cell Biosci* 9: 19.

1097 Zhao Y, Liang Y, Xu Z, Liu J, Liu X, Ma J, Sun C, Yang Y (2022) Exosomal miR-673-5p from
1098 fibroblasts promotes Schwann cell-mediated peripheral neuron myelination by targeting the
1099 TSC2/mTORC1/SREBP2 axis. *J Biol Chem* 298: 101718.

1100 Zhao Y, Liu J, Liu S, Yang P, Liang Y, Ma J, Mao S, Sun C, Yang Y (2023) Fibroblast
1101 exosomal TFAP2C induced by chitosan oligosaccharides promotes peripheral axon regeneration
1102 via the miR-132-5p/CAMKK1 axis. *Bioact Mater* 26: 249-263.

1103 Zou Y (2020) Breaking symmetry - cell polarity signaling pathways in growth cone guidance
1104 and synapse formation. *Curr Opin Neurobiol* 63: 77-86.
1105

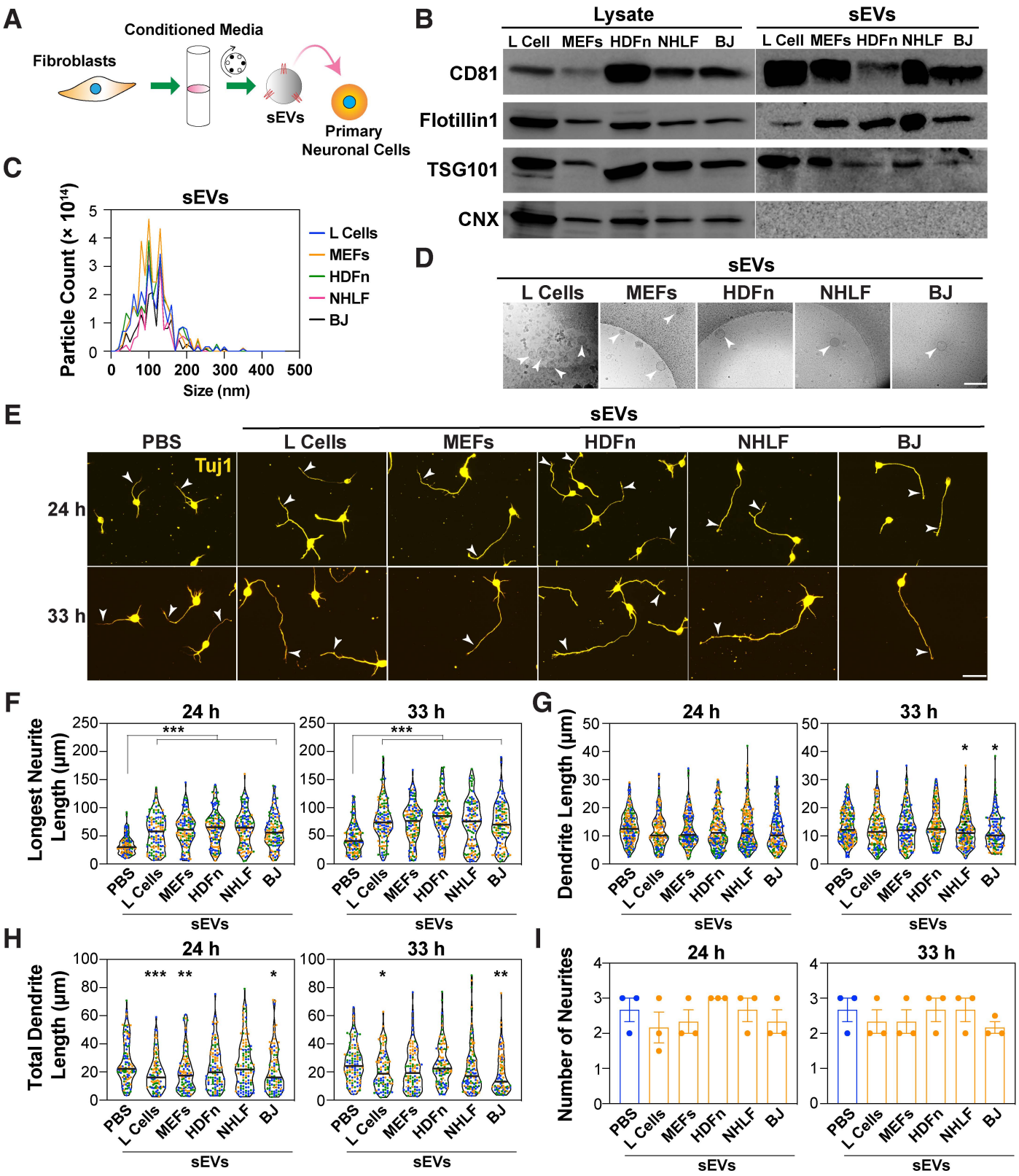
A
Conditioned Media
Fibroblasts
sEVs
Primary Neuronal Cells
B
Lysate
sEVs
L Cell MEFs HDFn NHLF BJ
L Cell MEFs HDFn NHLF BJ
CD81
Flotillin1
TSG101
CNX
C
sEVs
Particle Count (× 10^14)
Size (nm)
L Cells
MEFs
HDFn
NHLF
BJ
D
sEVs
L Cells MEFs HDFn NHLF BJ
E
sEVs
PBS L Cells MEFs HDFn NHLF BJ
Tuj1
24 h
33 h
F
24 h
33 h
Longest Neurite Length (µm)
PBS L Cells MEFs HDFn NHLF BJ
sEVs
G
24 h
33 h
Dendrite Length (µm)
H
24 h
33 h
Total Dendrite Length (µm)
I
24 h
33 h
Number of Neurites

Figure 1

Figure 1. sEVs promote the growth of the prospective axon. (A) A schematic of the experimental set up. Mouse cortical neurons (E15.5-16.5) are treated with sEVs isolated from fibroblast-conditioned media (CM) using differential centrifugation. (**B)** Representative immunoblotting of cell lysates and sEV pellets (100,000 x g) from the indicated fibroblast cell lines for EV markers CD81, Flotillin1 and TSG101 and the ER protein, calnexin (CNX). (**C)** Nanoparticle tracking analysis (NTA) of differential centrifugation pellets. A representative plot indicating the particle size distribution from 3 independent purifications is shown. (**D)** Representative transmission electron microscopy (TEM) images of sEV-containing pellets. Arrowheads indicate round vesicles. Scale bar, 200 nm. (**E-I)** Cortical neurons were treated with sEVs (5 µg/mL) purified from the indicated fibroblast cell lines, 4 h after plating. Neurons were fixed at 24 and 33 h, and neuronal morphology was examined after staining for Tuj1. **(E)** Representative images are shown. Arrowheads mark the longest neurite. Scale bar, 40 µm. **(F-I)** The length of the longest neurite (prospective axon; **F**), individual neurite/dendrite lengths **(G)**, total dendrite length (longest neurite excluded; **H**) and total number of neurites **(I)** were quantified from a minimum of 90 neurons per condition from 3 independent experiments. Neurite lengths are plotted as a violin plot with values from each experiment distinctly colored and the median marked by a black line **(F, G, H)**. The number of neurites are plotted as the average of the median ± SEM **(I)**, where each dot represents the median from 30 neurons from one of the three independent experiments. Statistical significance: *$p<0.05$, **$p<0.01$, ***$p<0.001$ using one-way ANOVA with Dunnett's post-test.

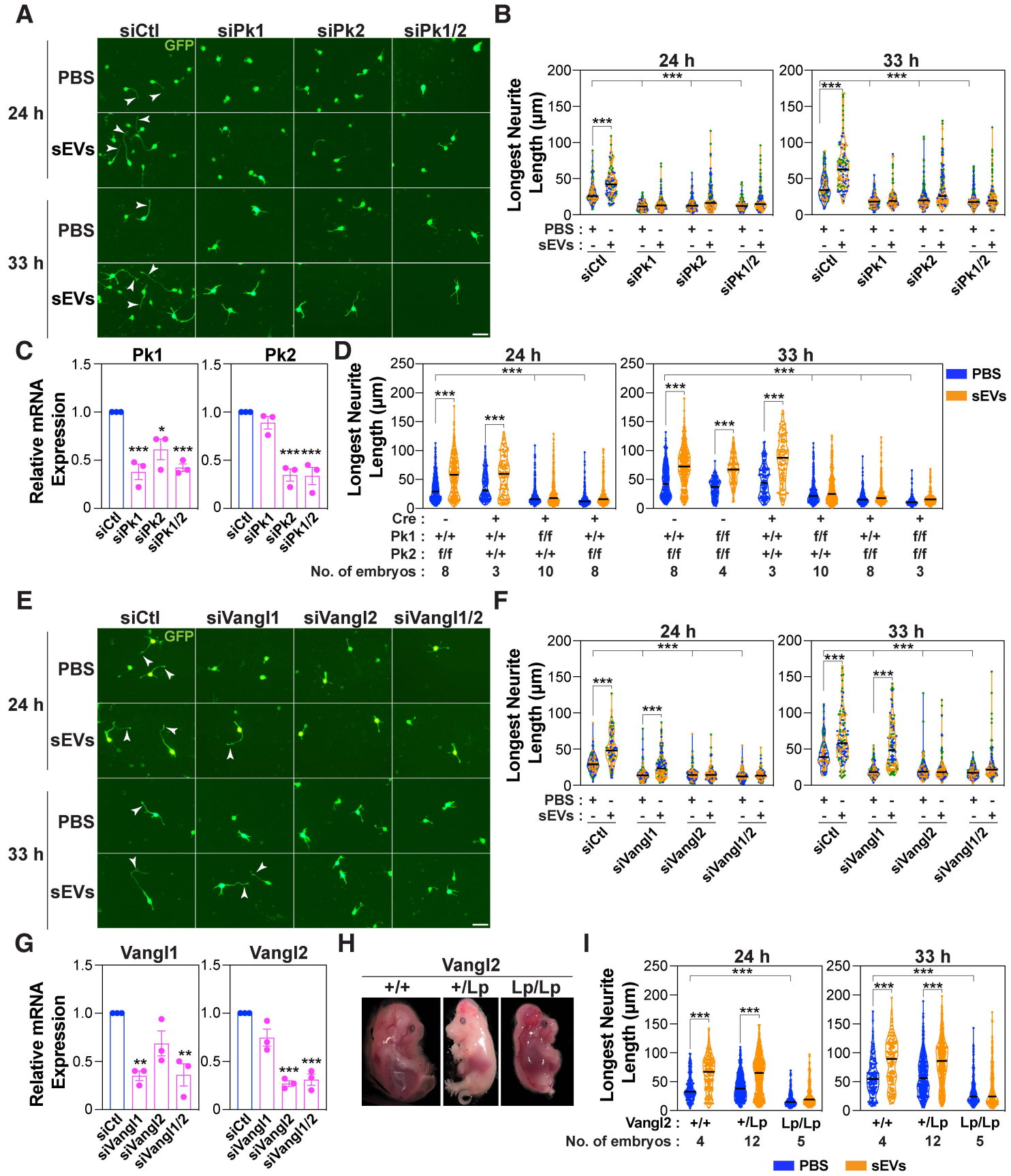
A
siCtl
siPk1
siPk2
siPk1/2
GFP
24 h
33 h
PBS
sEVs
B
24 h
33 h
Longest Neurite Length (μm)
PBS :
sEVs :
C
Pk1
Pk2
Relative mRNA Expression
D
Cre :
Pk1 :
Pk2 :
No. of embryos :
PBS
sEVs
E
siVangl1
siVangl2
siVangl1/2
F
G
Vangl1
Vangl2
H
+/+
+/Lp
Lp/Lp
I
Vangl2 :

Figure 2

Figure 2. The PCP components, Pk1/2 and Vangl2, are required for sEV-induced growth of the longest neurite. (A-C, E-G) Pk1/2 and Vangl2 promote sEV-induced neurite outgrowth. Dissociated E15.5-16.5 mouse cortical neurons were electroporated with siRNA against Pk1 (siPk1) and Pk2 (siPk2) (**A-C**), or Vangl1 (siVangl1) and Vangl2 (siVangl2) (**E-G**) individually or in combination or with siControl (siCtl) along with a GFP-expressing plasmid and were treated with sEVs (5 µg/mL) from L cells, 4 h after plating. Neurons were fixed at 24 and 33 h, and neuronal morphology was examined in GFP-positive neurons. (**A, E**) Representative images are shown. Arrowheads mark the longest neurite. Scale bar, 40 µm. (**B, F**) The length of the longest neurites was quantified. (**C, G)** Knockdown efficiency for Pk1/Pk2 (**C**) and Vangl1/2 (**G**) was determined in GFP-positive neurons isolated by FACS. Relative mRNA expression was determined by qPCR. (**D, I)** Pk1/2 and Vangl2 promote sEV-induced neurite outgrowth in mutant mouse models. Cortical neurons (E15.5-16.5) were isolated from Pk1 and Pk2 conditional knockout mice obtained by crossing Pk floxed mice with a Nestin-Cre line **(D)** or Vangl2 mutant littermates obtained by crossing of heterozygous loop-tail mutants (Vangl2$^{+/Lp}$) **(I).** Neurons were treated with sEVs from L cells, 4 h after plating, fixed at 24 and 33 h and morphology examined in Tuj1 stained neurons. The length of the longest neurite was quantified from 40 neurons per embryo, and total number of embryos analyzed are indicated below the genotypes. Violin plots with the median marked by a black line are shown. **(H)** Loop-tail embryos exhibit an open neural tube. Representative images are shown from a minimum 4 independent experiments.

In siRNA experiments, neurite lengths are quantified from a minimum of 90 neurons per condition from 3 independent experiments and plotted as a violin plot with values from each experiment distinctly colored and the median marked by a black line **(B, F**). For qPCR plots, data is presented as the mean ± SEM from 3 independent experiments **(C, G)**. Statistical significance: *$p<0.05$, **$p<0.01$, ***$p<0.001$ using one-way ANOVA with Dunnett's post-test **(C, G)**, or two-way ANOVA with Tukey's post-test **(B, D, F, I)**.

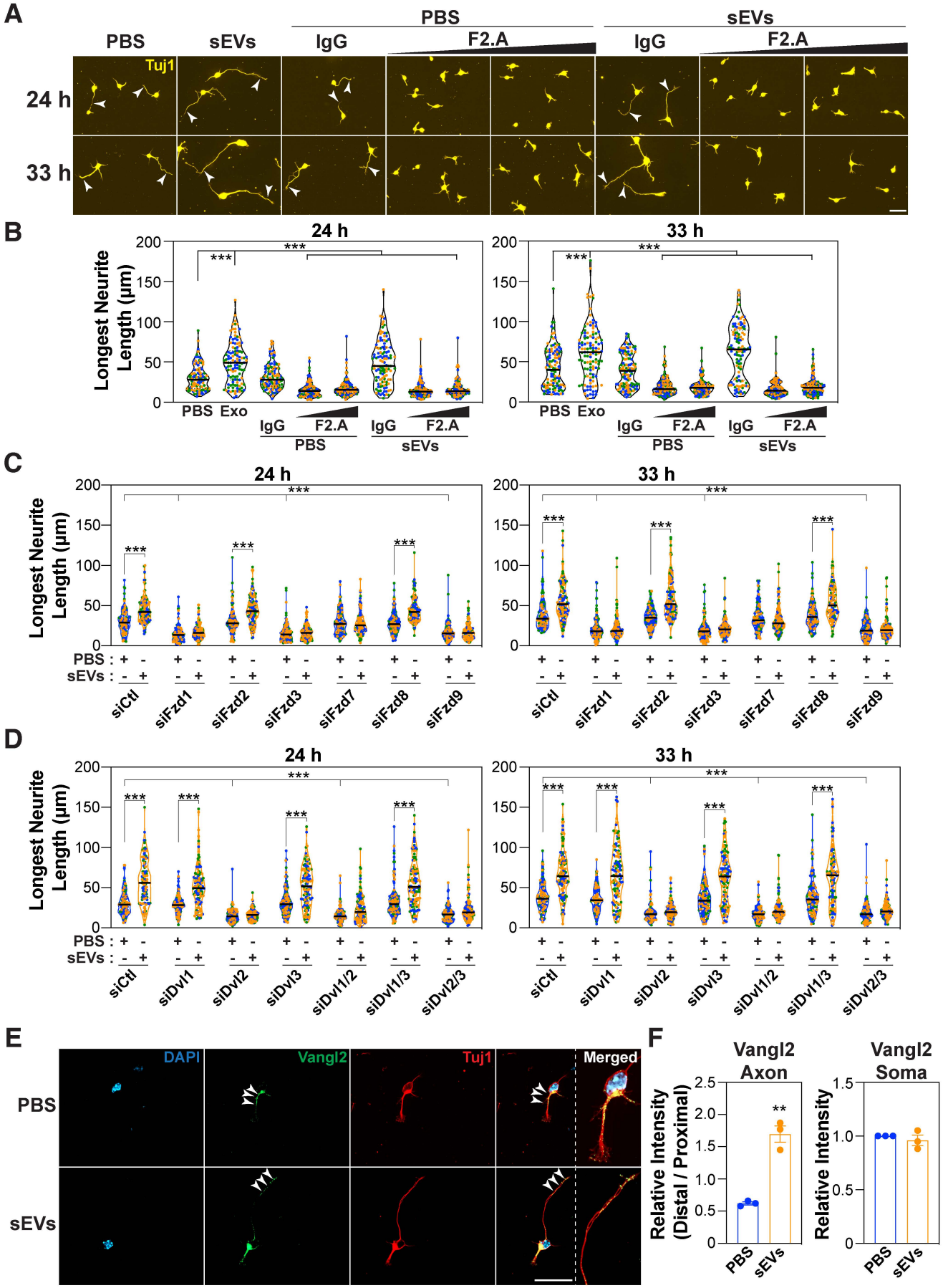
A
PBS
sEVs
IgG
F2.A
Tuj1
24 h
33 h
B
Longest Neurite Length (µm)
Exo
C
siCtl
siFzd1
siFzd2
siFzd3
siFzd7
siFzd8
siFzd9
D
siDvl1
siDvl2
siDvl3
siDvl1/2
siDvl1/3
siDvl2/3
E
DAPI
Vangl2
Merged
F
Vangl2 Axon
Vangl2 Soma
Relative Intensity (Distal / Proximal)
Relative Intensity

Figure 3

Figure 3. Fzds and Dvls are required for sEV-induced growth of the longest neurite. (A-D) Dissociated E15.5-16.5 mouse cortical neurons were treated with sEVs (5 µg/mL) from L cells, 4 h after plating. **(A-B)** Neurons were co-treated with IgG or a Fzd blocking antibody, F2.A (at 50 nM and 100 nM) along with sEVs. **(C-D)** Neurons were electroporated with siRNA against Fzds (siFzds) **(C)**, or Dvls (siDvl) **(D)** or siControl in combination with a GFP-expressing plasmid prior to the addition of sEVs. Neurons were fixed at 24 and 33 h, and neuronal morphology was examined in Tuj1 stained **(A, B)** or GFP-positive neurons **(C, D)** with representative images shown. Arrowheads mark the longest neurite. Scale bar, 40 µm. **(B-D)** The length of the longest neurite was quantified. **E)** sEVs promote localization of Vangl2 to the distal axon. Cortical neurons were treated with sEVs from L cells, 4 h after plating and fixed after 24 h. Representative confocal images of neurons stained with DAPI (blue), Vangl2 (green) and Tuj1 (red) are shown. Arrowheads mark the Vangl2 localization. (**F)** The ratio of distal/proximal Vangl2 intensity and the relative intensity of Vangl2 in soma is quantified from 30 neurons from 3 independent experiments.

Neurite lengths are quantified from a minimum of 90 neurons per condition from 3 independent experiments and plotted as a violin plot with values from each experiment distinctly colored and the median marked by a black line **(B, C, D)**. For Vangl2 plots, data is presented as the mean ± SEM from 3 independent experiments **(F)**. Statistical significance: **$p<0.01$, ***$p<0.001$ using unpaired t-test **(F)**, one-way ANOVA with Dunnett's post-test **(B)**, or two-way ANOVA with Tukey's post-test **(C, D)**.

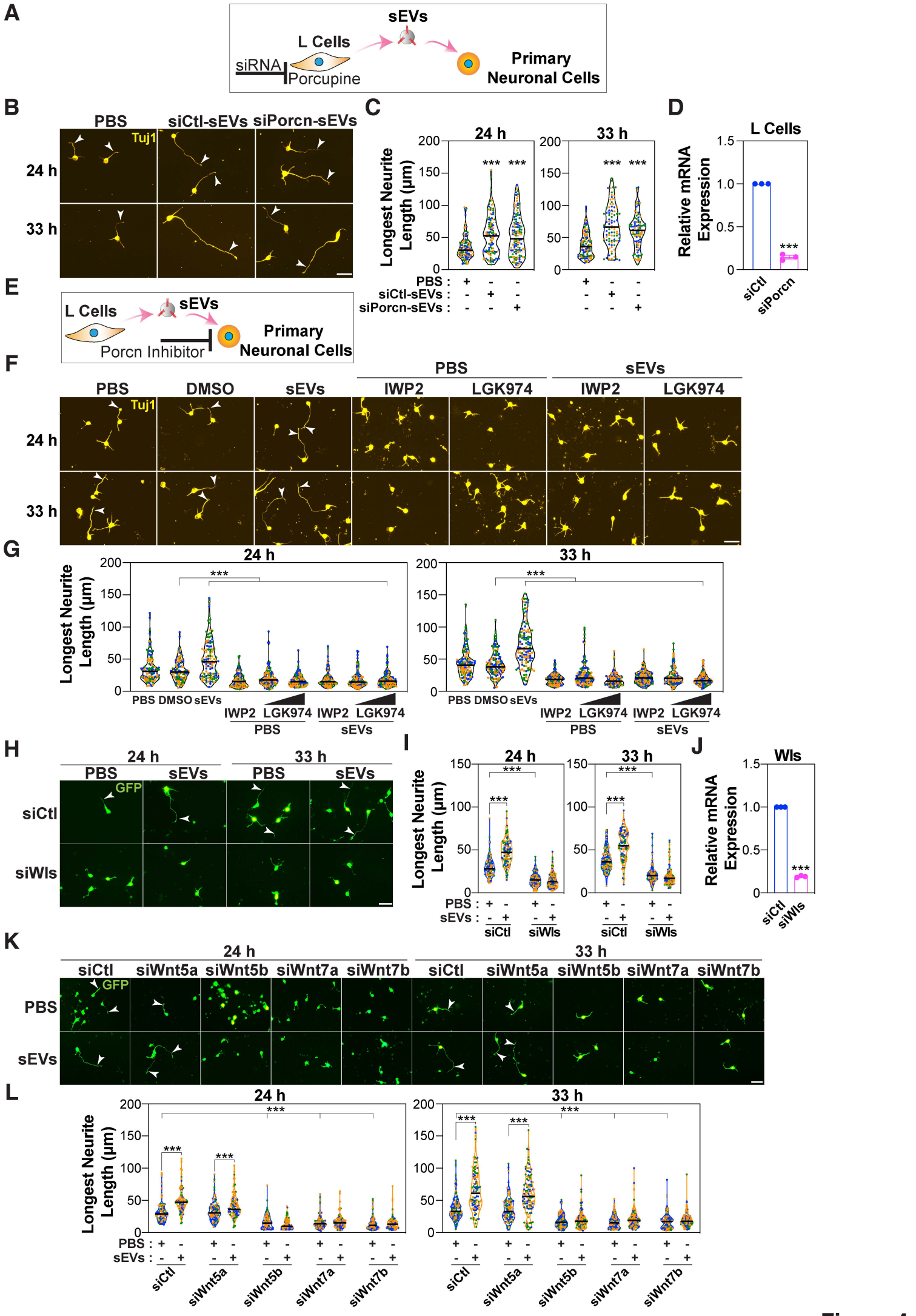
A
sEVs
L Cells
siRNA
Porcupine
Primary Neuronal Cells
B
PBS
siCtl-sEVs
siPorcn-sEVs
Tuj1
24 h
33 h
C
24 h
33 h
Longest Neurite Length (μm)
PBS :
siCtl-sEVs :
siPorcn-sEVs :
D
L Cells
Relative mRNA Expression
siCtl
siPorcn
E
L Cells
sEVs
Porcn Inhibitor
Primary Neuronal Cells
F
PBS
DMSO
sEVs
IWP2
LGK974
G
PBS DMSO sEVs
IWP2 LGK974 IWP2 LGK974
PBS
sEVs
H
siCtl
siWls
GFP
I
sEVs :
J
Wls
K
siWnt5a
siWnt5b
siWnt7a
siWnt7b
L

Figure 4

Figure 4. Neuronal Wnts mediates sEV-induced growth of the longest neurite. (A, E) Schematics, illustrating the experimental set up. **(A-G)** Dissociated E15.5-16.5 mouse cortical neurons are treated with sEVs isolated from L cells transfected with siCtl or siPorcupine **(A-D)** or with sEVs isolated from regular L cells. Neurons were treated with PBS as control and with porcupine (Porcn) inhibitors, IWP2 (10 μM) or LGK974 (1 and 5 μM) **(E-G)**, 4 h after plating and were co-incubated with sEVs. (**H-L)** Cortical neurons were electroporated with siRNAs against Wls (siWls) **(H, I)** or Wnts (siWnts) **(K, L)** or siControl (siCtl) along with a GFP-expressing plasmid and then treated with sEVs (5 μg/mL) from L cells, 4 h after plating. Neurons were fixed at 24 and 33 h, and neuronal morphology was examined in Tuj1 stained neurons **(B, C, F, G)** or GFP-positive neurons for siRNA experiments **(H, I, K, L)**. Representative images **(B, F, H, K)** and quantifications of the longest neurite **(C, G, I, L)** are shown. (**D, J)** Knockdown efficiency for porcupine **(D)** and Wls **(J)** was determined in L cells and GFP-positive neurons isolated by FACS, respectively. Relative mRNA expression was determined by qPCR.

Neurite lengths are quantified from a minimum of 90 neurons per condition from 3 independent experiments and plotted as a violin plot with values from each experiment distinctly colored and the median marked by a black line **(C, G, I, L)**. For all other plots, data is presented as the mean ± SEM from 3 independent experiments **(D, J)**. Statistical significance: ***$p<0.001$ using unpaired t-test **(D, J)**, one-way ANOVA with Dunnett's post-test **(C, G)**, or two-way ANOVA with Tukey's post-test **(I, L)**.

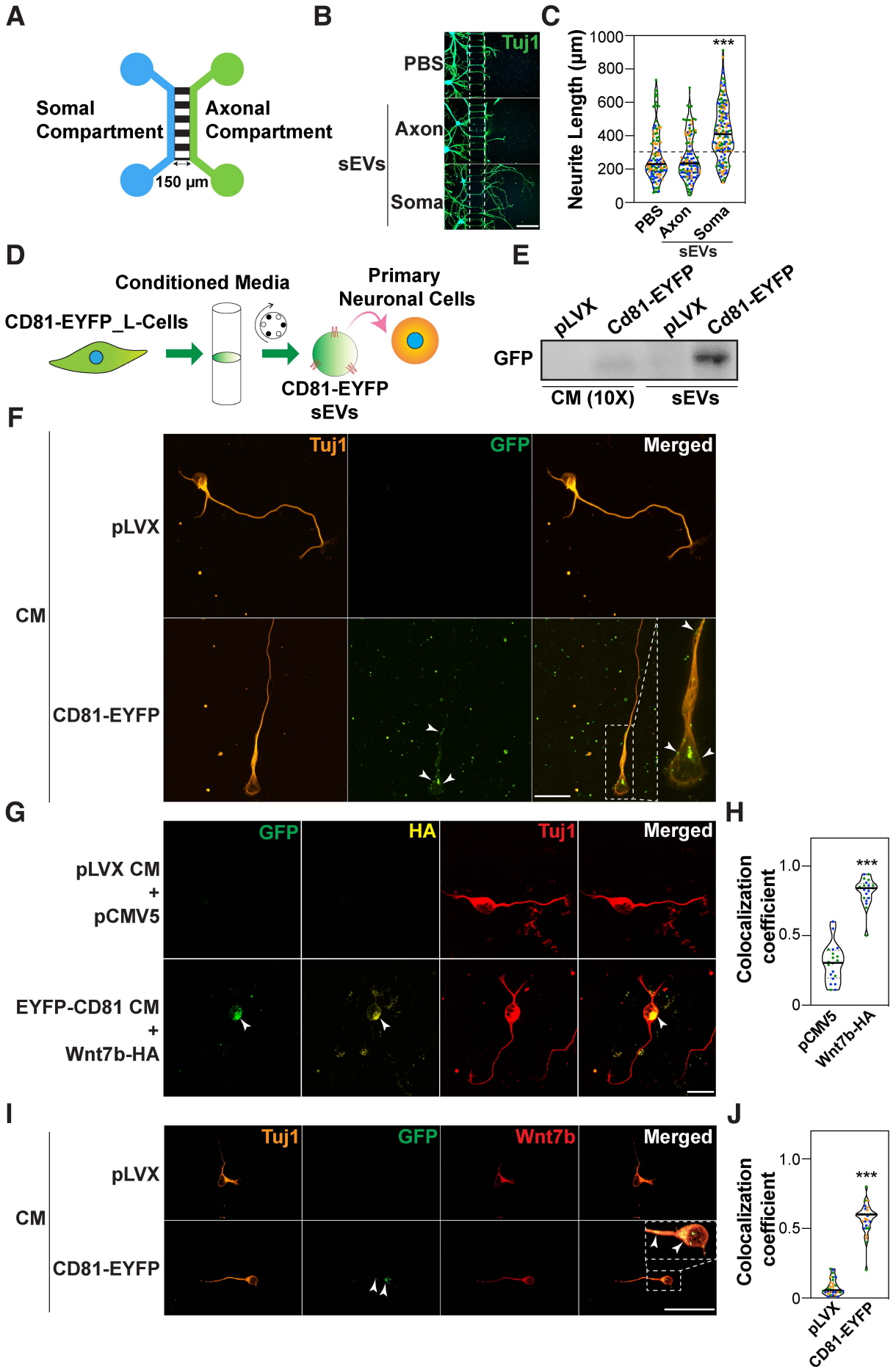
A
Somal Compartment
Axonal Compartment
150 µm
B
Tuj1
PBS
sEVs
Axon
Soma
C
Neurite Length (µm)
1000
800
600
400
200
0
***
PBS
Axon
Soma
sEVs
D
Conditioned Media
CD81-EYFP_L-Cells
Primary Neuronal Cells
CD81-EYFP sEVs
E
pLVX
Cd81-EYFP
pLVX
Cd81-EYFP
GFP
CM (10X)
sEVs
F
Tuj1
GFP
Merged
pLVX
CM
CD81-EYFP
G
GFP
HA
Tuj1
Merged
pLVX CM + pCMV5
EYFP-CD81 CM + Wnt7b-HA
H
Colocalization coefficient
1.0
0.5
0
***
pCMV5
Wnt7b-HA
I
Tuj1
GFP
Wnt7b
Merged
pLVX
CM
CD81-EYFP
J
Colocalization coefficient
1.0
0.5
0
***
pLVX
CD81-EYFP

Figure 5

Figure 5. sEVs promote neurite elongation and co-localize with Wnt7b. (A-C) sEVs promote neurite elongation. **(A)** A schematic illustration of the two compartment Xona microfluidic device. The somal compartment is connected to axonal compartment through a 150 μm microgroove. **(B)** Cortical neurons (E15.5-16.5) were seeded in the somal compartment and cultured for 5 days prior to the addition of the L cell-derived sEVs in either the somal or axonal compartment. Neurons were fixed 24 h later and neuronal morphology was examined in Tuj1 stained neurons. Representative images are shown. Scale bar, 200 μm. **(C)** The length of the neurites growing in the microgroove and emerging in the axonal compartment was quantified for a minimum of 90 neurites. A dotted line marks both ends of the microgroove (150 μm). **(D-I)** sEVs can be internalized by neurons and associate with Wnts. Cortical neurons were treated with 10X concentrated conditioned media (CM) from L cells stably expressing CD81-EYFP, 4 h after plating for 29 h **(F)** or 24 h after plating for 30 min **(G, I)**. In panel **G**, cortical neurons were electroporated with 2 μg of either pCMV5 or C-terminal HA-tagged Wnt7b (Wnt7b-HA). Representative images of neurons immunostained with GFP and Tuj1 **(F, I)** or GFP, Tuj1 and HA **(G)** are shown. Scale bar, 20 μm **(F, G)** or 40 μm **(I)**. **(E)** Characterization of sEVs. The concentrated CM (10X) and sEV pellet from L cells were immunoblotted with anti-GFP antibody. **(H, J)** Pearson's colocalization coefficient for **(G)** and **(I)**. Neurons were identified using Tuj1 as a reference channel and the colocalization coefficient was quantified using Nikon NIS-Elements software.

Images **(F, I)** and the quantification **(J)** are representative of 30 neurons from 3 independent experiments or 20 neurons from 2 independent experiments **(G, H)**. In all the violin plots, values are distinctly colored for each experiment and the median marked by a black line. Statistical significance: ***$p<0.001$ using unpaired t-test **(H, J)** or one-way ANOVA with Dunnett's post-test **(C)**.

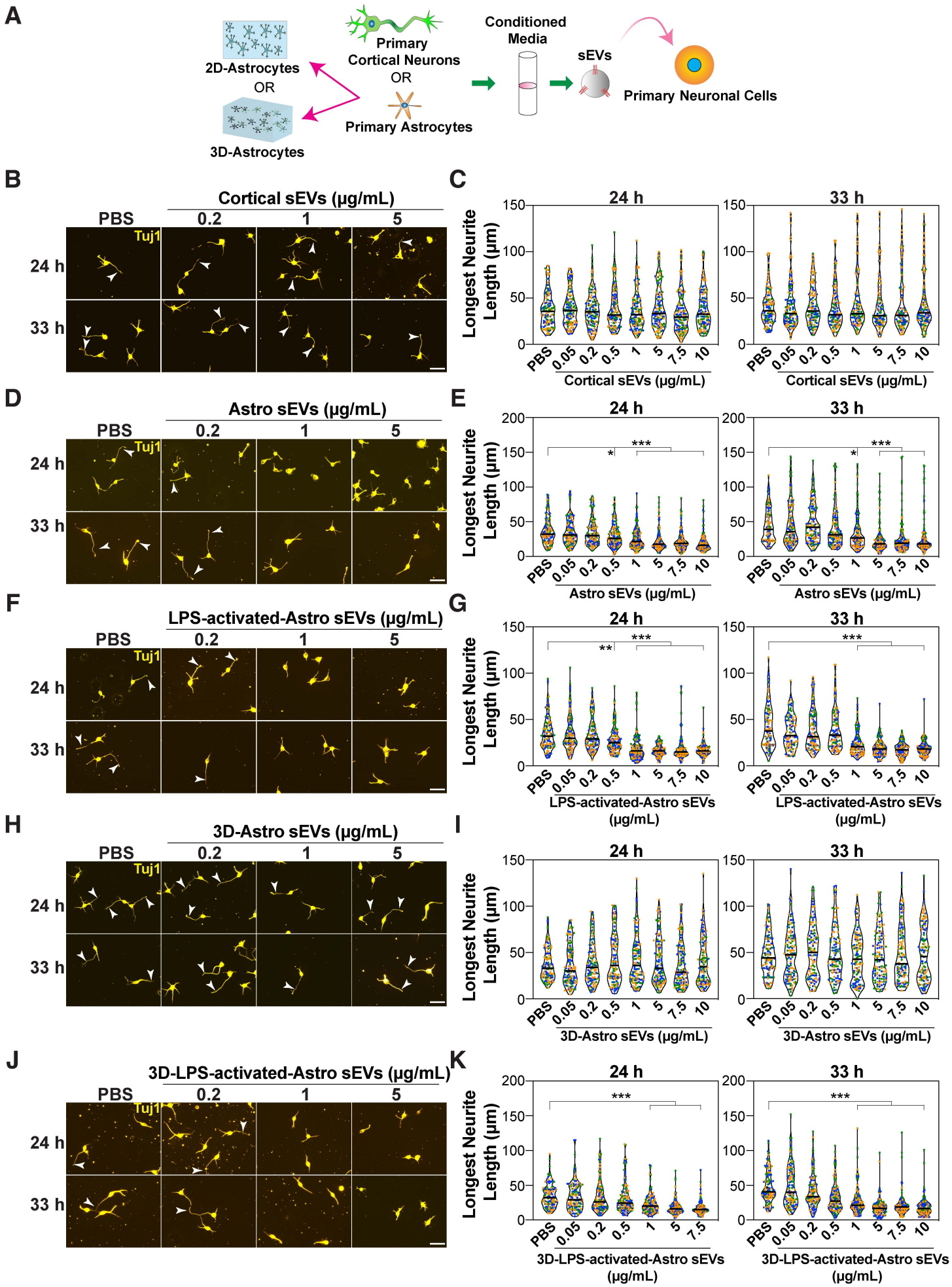
A
2D-Astrocytes
OR
3D-Astrocytes
Primary
Cortical Neurons
OR
Primary Astrocytes
Conditioned
Media
sEVs
Primary Neuronal Cells
B
Cortical sEVs (µg/mL)
PBS
0.2
1
5
Tuj1
24 h
33 h
C
24 h
33 h
Longest Neurite
Length (µm)
PBS
0.05
0.2
0.5
1
5
7.5
10
Cortical sEVs (µg/mL)
D
Astro sEVs (µg/mL)
E
Astro sEVs (µg/mL)
F
LPS-activated-Astro sEVs (µg/mL)
G
LPS-activated-Astro sEVs
(µg/mL)
H
3D-Astro sEVs (µg/mL)
I
3D-Astro sEVs (µg/mL)
J
3D-LPS-activated-Astro sEVs (µg/mL)
K
3D-LPS-activated-Astro sEVs
(µg/mL)

Figure 6

Figure 6. sEVs from neurons and astrocytes do not promote growth of the longest neurite. **(A)** A schematic illustration of the experimental set up. Dissociated E15.5-16.5 cortical neurons were treated with sEVs purified from primary cortical neurons or primary astrocytes. **(B-K)** Cortical neurons were treated with various concentrations (0.05-10 μg/mL) of sEVs purified from cortical neurons **(B, C),** astrocytes **(D, E),** LPS-activated astrocytes **(F, G),** 3D-astrocytes grown in collagen gel **(H, I)** and LPS-activated 3D-astrocytes **(J, K)**, 4 h after plating. Neurons were fixed at 24 and 33 h, and neuronal morphology was examined in Tuj1 stained neurons. Representative images (**B, D, F, H, J**) and quantifications (**C, E, G, I, K**) are shown. Arrowheads mark the longest neurite. Scale bar, 40 μm.

Neurite lengths are quantified from a minimum of 90 neurons per condition from 3 independent experiments and plotted as a violin plot with values from each experiment distinctly colored and the median marked by a black line. Statistical significance: *$p<0.05$, **$p<0.01$, ***$p<0.001$ using one-way ANOVA with Dunnett's post-test.

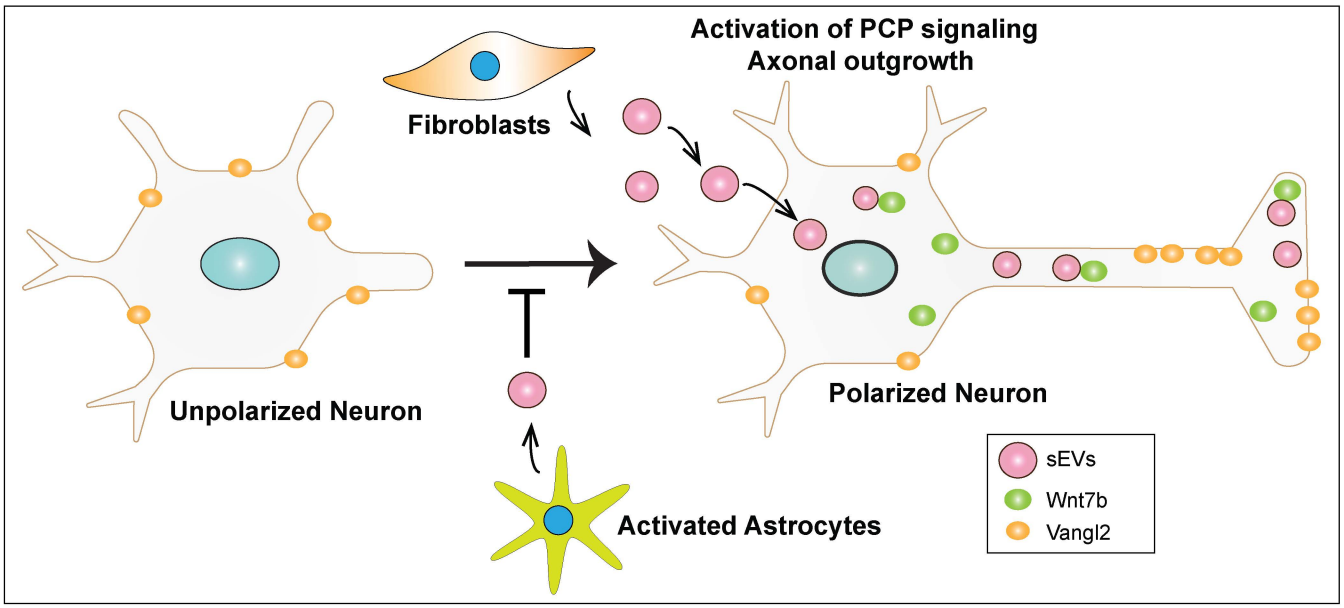

Figure 7. A model, depicting the effect of sEVs in promoting axon outgrowth and polarized neuronal morphology through Wnt-PCP signaling. sEVs secreted by L cells engage Wnt-PCP signaling in neurons to promote axon outgrowth that results in the acquisition of a polarized neuronal morphology. sEVs induce a shift in Vangl2 localization towards distal axon. sEVs can be internalized by neurons and can co-localize with Wnt7b to promote the growth of the prospective axon. In contrast to fibroblast derived sEVs, those isolated from activated astrocytes inhibit neurite outgrowth.

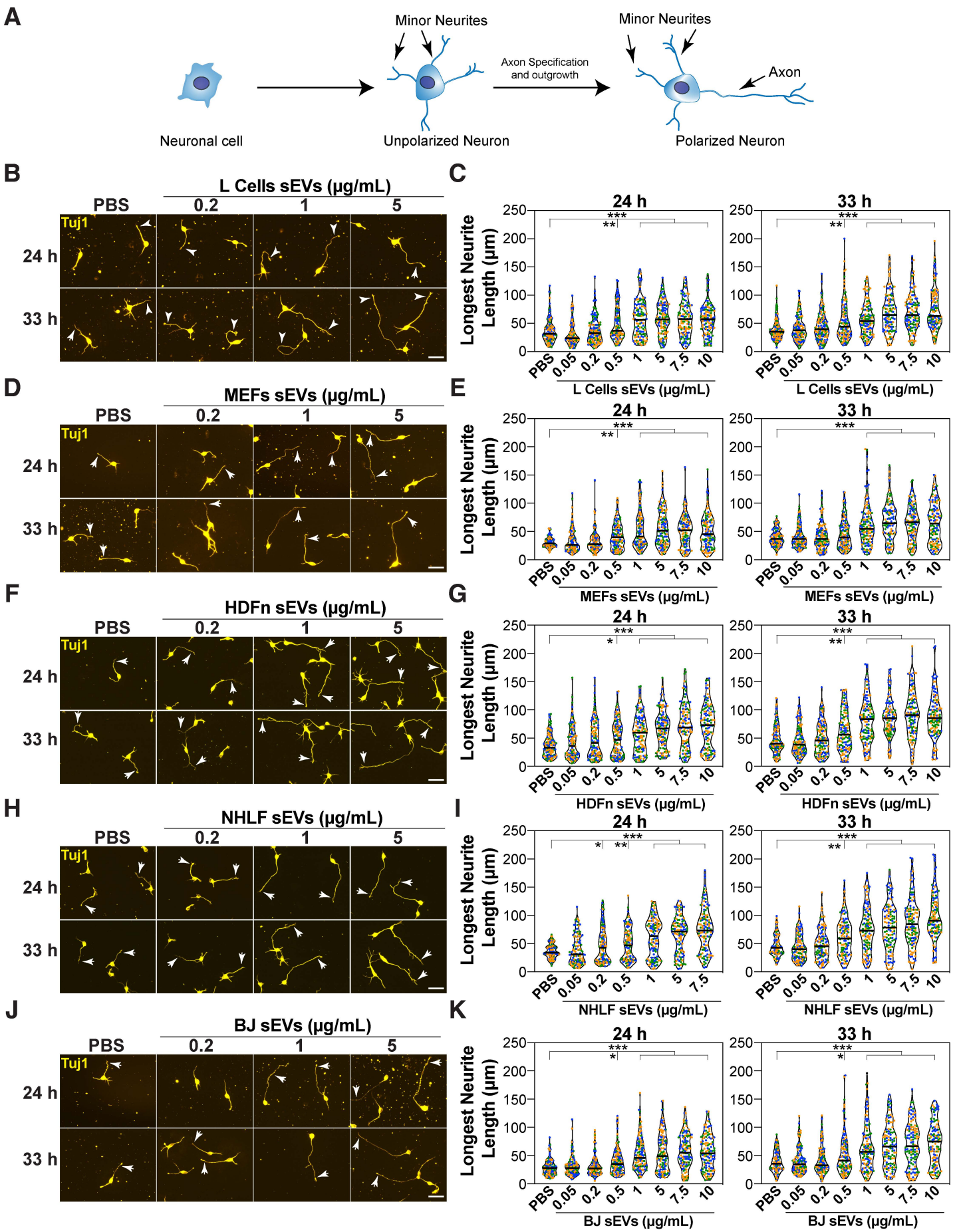
A
Minor Neurites
Minor Neurites
Axon Specification and outgrowth
Axon
Neuronal cell
Unpolarized Neuron
Polarized Neuron
B
L Cells sEVs (µg/mL)
PBS
0.2
1
5
Tuj1
24 h
33 h
C
24 h
33 h
Longest Neurite Length (µm)
L Cells sEVs (µg/mL)
D
MEFs sEVs (µg/mL)
E
MEFs sEVs (µg/mL)
F
HDFn sEVs (µg/mL)
G
HDFn sEVs (µg/mL)
H
NHLF sEVs (µg/mL)
I
NHLF sEVs (µg/mL)
J
BJ sEVs (µg/mL)
K
BJ sEVs (µg/mL)
PBS
0.05
0.2
0.5
1
5
7.5
10

Figure S1

Figure S1. sEVs promote the growth of the longest neurite in a concentration-dependent manner. Related to Fig. 1. (A) A schematic of the morphological changes in neurons cultured *in vitro*. **(B-K)** Dissociated E15.5-16.5 mouse cortical neurons were treated with various concentrations (0.05-10 μg/mL) of sEVs purified from the indicated fibroblast cell lines including L cells **(B, C)**, MEFs **(D, E)**, HDFn **(F, G)**, NHLF **(H, I)** and BJ **(J, K),** 4 h after plating. Neurons were fixed at 24 and 33 h, and neuronal morphology was examined in Tuj1 stained neurons. Representative images **(B, D, F, H, J)** and quantifications **(C, E, G, I, K)** are shown. Arrowheads mark the longest neurite. Scale bar, 40 μm.

Neurite lengths are quantified from a minimum of 90 neurons per condition from 3 independent experiments and plotted as a violin plot with values from each experiment distinctly colored and the median marked by a black line. Statistical significance: *$p<0.05$, **$p<0.01$, ***$p<0.001$ using one-way ANOVA with Dunnett's post-test.

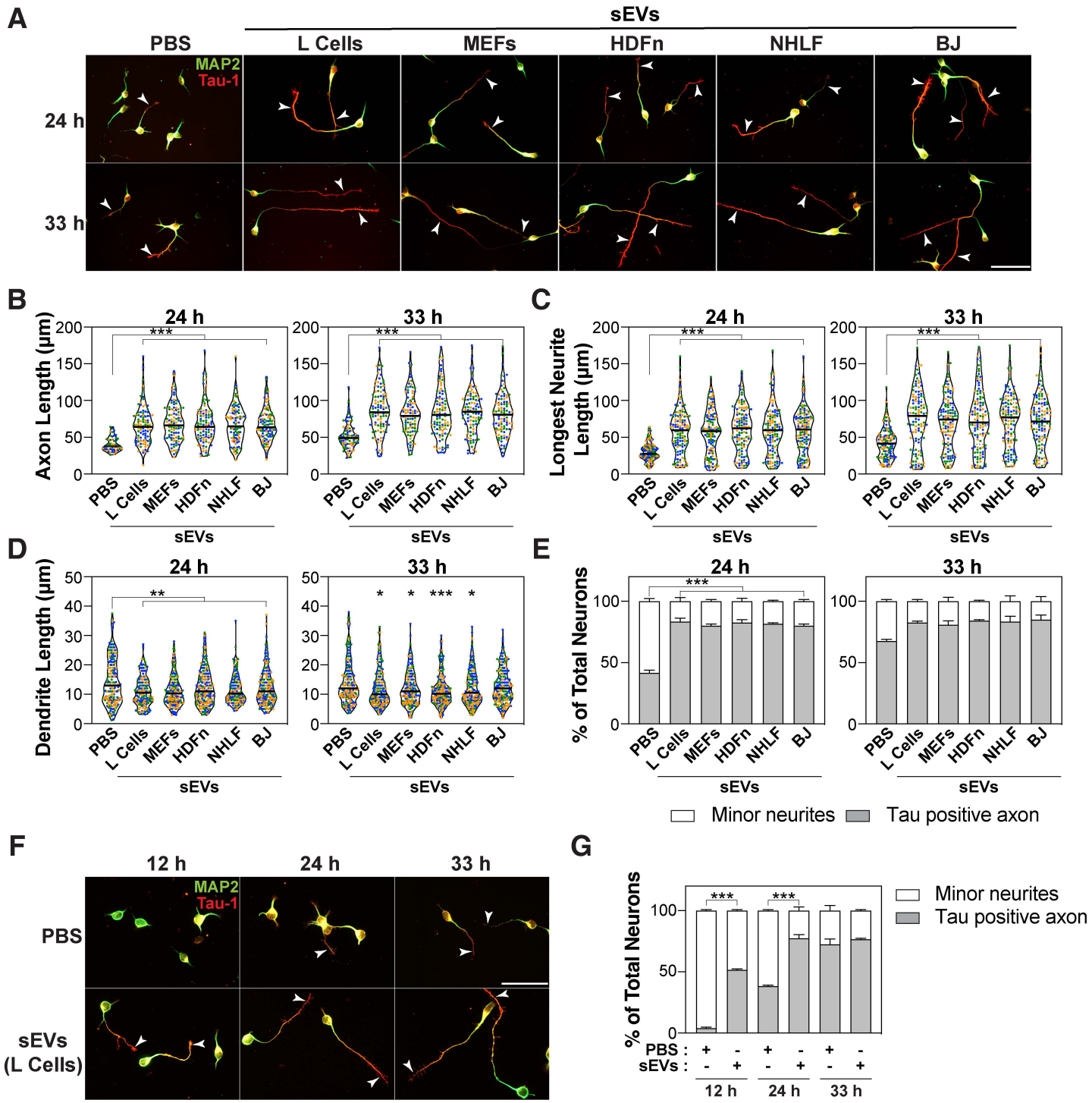
A
sEVs
PBS
L Cells
MEFs
HDFn
NHLF
BJ
MAP2
Tau-1
24 h
33 h
B
Axon Length (µm)
24 h
33 h
***
PBS
L Cells
MEFs
HDFn
NHLF
BJ
sEVs
C
Longest Neurite Length (µm)
D
Dendrite Length (µm)
**
*
***
E
% of Total Neurons
Minor neurites
Tau positive axon
F
12 h
24 h
33 h
PBS
sEVs (L Cells)
G
% of Total Neurons
PBS :
sEVs :
12 h
24 h
33 h

Figure S2

Figure S2. sEVs promote axon outgrowth and polarized neuronal morphology. Related to Fig. 1. (**A-G)** Dissociated E15.5-16.5 mouse cortical neurons were treated with sEVs purified from the indicated fibroblast cell lines **(A-E)** or only L cells **(F-G)**, 4 h after plating. Neurons were fixed at 24 and 33 h **(A-E)** or 12, 24 and 33 h **(F-G)**, and neuronal morphology was examined in neurons immunostained for MAP2 (dendrites, green) and Tau-1 (axons, red). **(A, F)** Representative images are shown. Arrowheads mark Tau-1 positive axons. Scale bar, 50 µm. (**B-E**) The length of the Tau-1 positive axons **(B)**, longest neurite (independent of Tau-1+ staining, **C**) and individual dendrite length (MAP2 positive, **D**) is quantified. (**E, G)** Percent of neurons containing only minor neurites (MAP2 positive) or a single Tau-1-positive axon, is plotted.

Neurite lengths are quantified from a minimum of 45 (for 24 h in panel **B**) or 90 (for all others) neurons per condition from 3 independent experiments and plotted as a violin plot with values from each experiment distinctly colored and the median marked by a black line. In panel **B**, for the 24 h control group (PBS treated), less data points were available due to greater percentage of neurons lacking a Tau-1 positive axon. Statistical significance: *$p<0.05$, **$p<0.01$, ***$p<0.001$ using one-way ANOVA with Dunnett's post-test **(B, C, D)**, or two-way ANOVA with Tukey's post-test **(E, G)**.

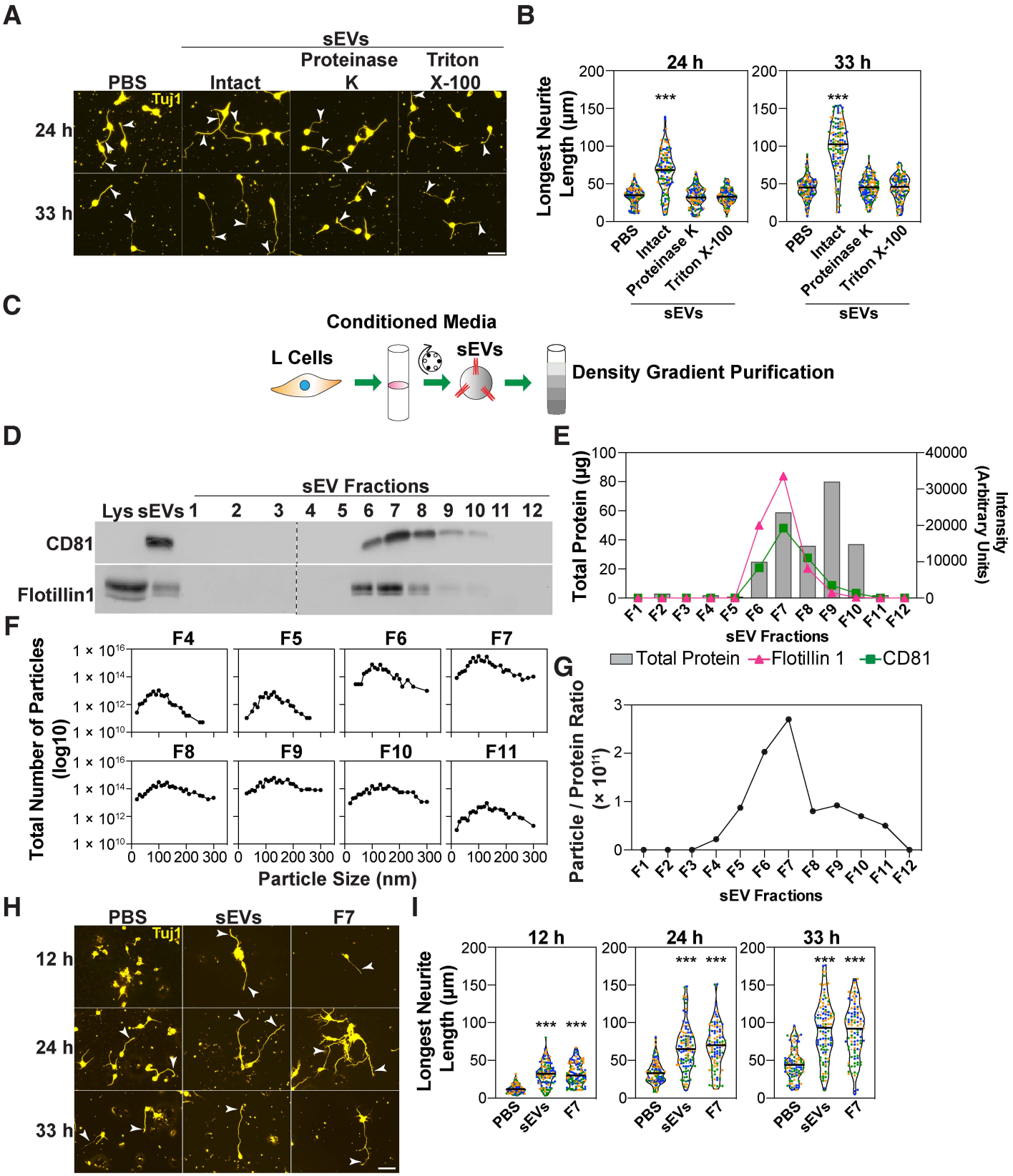
A
sEVs
PBS
Intact
Proteinase K
Triton X-100
Tuj1
24 h
33 h
B
24 h
33 h
Longest Neurite Length (µm)
***
PBS
Intact
Proteinase K
Triton X-100
sEVs
C
Conditioned Media
L Cells
sEVs
Density Gradient Purification
D
sEV Fractions
Lys sEVs 1 2 3 4 5 6 7 8 9 10 11 12
CD81
Flotillin1
E
Total Protein (µg)
Intensity (Arbitrary Units)
sEV Fractions
F1 F2 F3 F4 F5 F6 F7 F8 F9 F10 F11 F12
Total Protein
Flotillin 1
CD81
F
F4 F5 F6 F7
F8 F9 F10 F11
Total Number of Particles (log10)
Particle Size (nm)
G
Particle / Protein Ratio (× 10^11)
sEV Fractions
H
PBS
sEVs
F7
Tuj1
12 h
24 h
33 h
I
12 h
24 h
33 h
Longest Neurite Length (µm)
PBS
sEVs
F7

Figure S3

Figure S3. sEVs isolated using a discontinuous density gradient promote the growth of the longest neurite. Related to Fig. 1. (A-B, H-I) Dissociated E15.5-16.5 cortical neurons were treated with the intact sEVs, Proteinase K treated and Triton X-100 treated sEV pellet **(A-B)** or sEV pellet and the F7 fraction (both at 2×10^8 particles/mL) **(H-I)**, 4 h after plating. Neuronal morphology was examined in Tuj1 stained neurons at 24 and 33 h **(A-B)** or 12, 24 and 33 h **(H-I)**. Representative images **(A, H)** and quantifications **(B, I)** are shown. Arrowheads mark the longest neurite. Scale bar, 40 µm. **(C)** A schematic of the experimental set up. sEV pellets (100,000 x g) purified from the conditioned media (CM) of L cells using differential centrifugation were subjected to iodixanol discontinuous density gradient purification. (**D)** Twelve fractions were collected starting from the top of the discontinuous gradient and were analyzed by immunoblotting for the indicated EV markers. (**E)** Intensity of the bands of EV markers from **(D)** is plotted against the protein concentration. (**F)** Particle size distribution was determined using NTA. (**G)** Fraction 7 (F7) has the highest particle number/protein ratio.
Neurite lengths are quantified from a minimum of 90 neurons per condition from 3 independent experiments and plotted as a violin plot with values from each experiment distinctly colored and the median marked by a black line. Statistical significance: ***$p<0.001$ using one-way ANOVA with Dunnett's post-test.

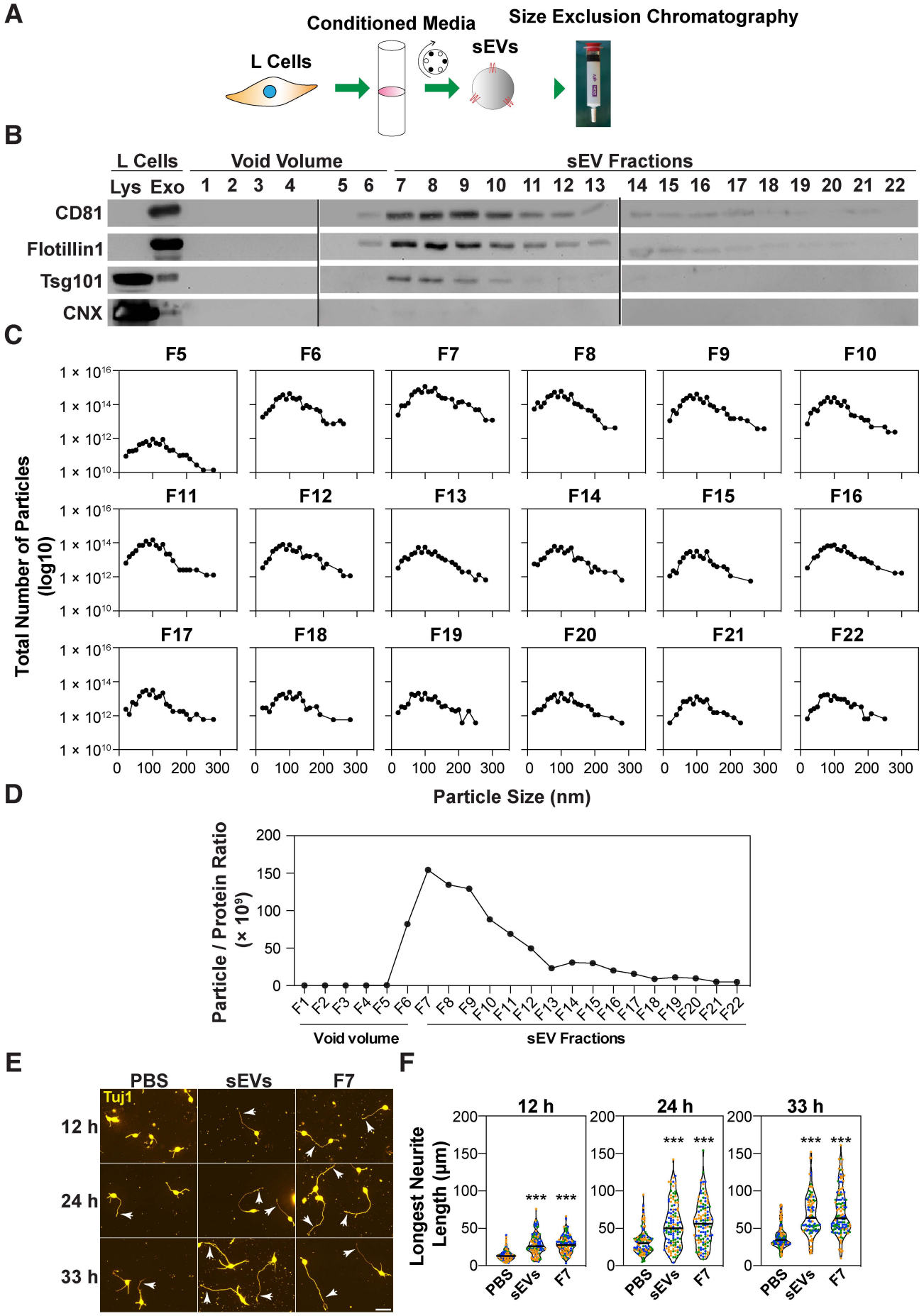
A
Conditioned Media
Size Exclusion Chromatography
L Cells
sEVs
B
L Cells
Void Volume
sEV Fractions
Lys Exo 1 2 3 4 5 6 7 8 9 10 11 12 13 14 15 16 17 18 19 20 21 22
CD81
Flotillin1
Tsg101
CNX
C
F5 F6 F7 F8 F9 F10
F11 F12 F13 F14 F15 F16
F17 F18 F19 F20 F21 F22
Total Number of Particles (log10)
1 × 10^16
1 × 10^14
1 × 10^12
1 × 10^10
0 100 200 300
Particle Size (nm)
D
Particle / Protein Ratio (× 10^9)
200
150
100
50
0
F1 F2 F3 F4 F5 F6 F7 F8 F9 F10 F11 F12 F13 F14 F15 F16 F17 F18 F19 F20 F21 F22
Void volume
sEV Fractions
E
PBS
sEVs
F7
Tuj1
12 h
24 h
33 h
F
12 h
24 h
33 h
Longest Neurite Length (µm)
200
150
100
50
0
***
PBS
sEVs
F7

Figure S4

Figure S4. sEVs isolated using size exclusion chromatography promote the growth of the longest neurite. Related to Fig. 1. (A) A schematic illustration of experimental setup. sEVs purified from the CM of L cells were subjected to size exclusion chromatography. **(B)** A total of 22 fractions were collected and subjected to immunoblotting for EV markers. (**C**) Particle size was measured using NTA. **(D)** Fraction 7 (F7) has the highest particle number/protein ratio. **(E)** F7 fraction promotes the growth of the longest neurite. Dissociated E15.5-16.5 cortical neurons were treated with resuspended sEV pellet (5 μg/mL) and F7 fraction (5 μg/mL), 4 h after plating. Neuronal morphology was examined in Tuj1 stained neurons at various time points: 12, 24 and 33 h. Representative images are shown. Arrowheads mark the longest neurite. Scale bar, 40 μm. **(F)** The length of the longest neurite was quantified from a minimum of 90 neurons per condition from 3 independent experiments and plotted as a violin plot with values from each experiment distinctly colored and the median marked by a black line. Statistical significance: ***$p<0.001$ using one-way ANOVA with Dunnett's post-test.

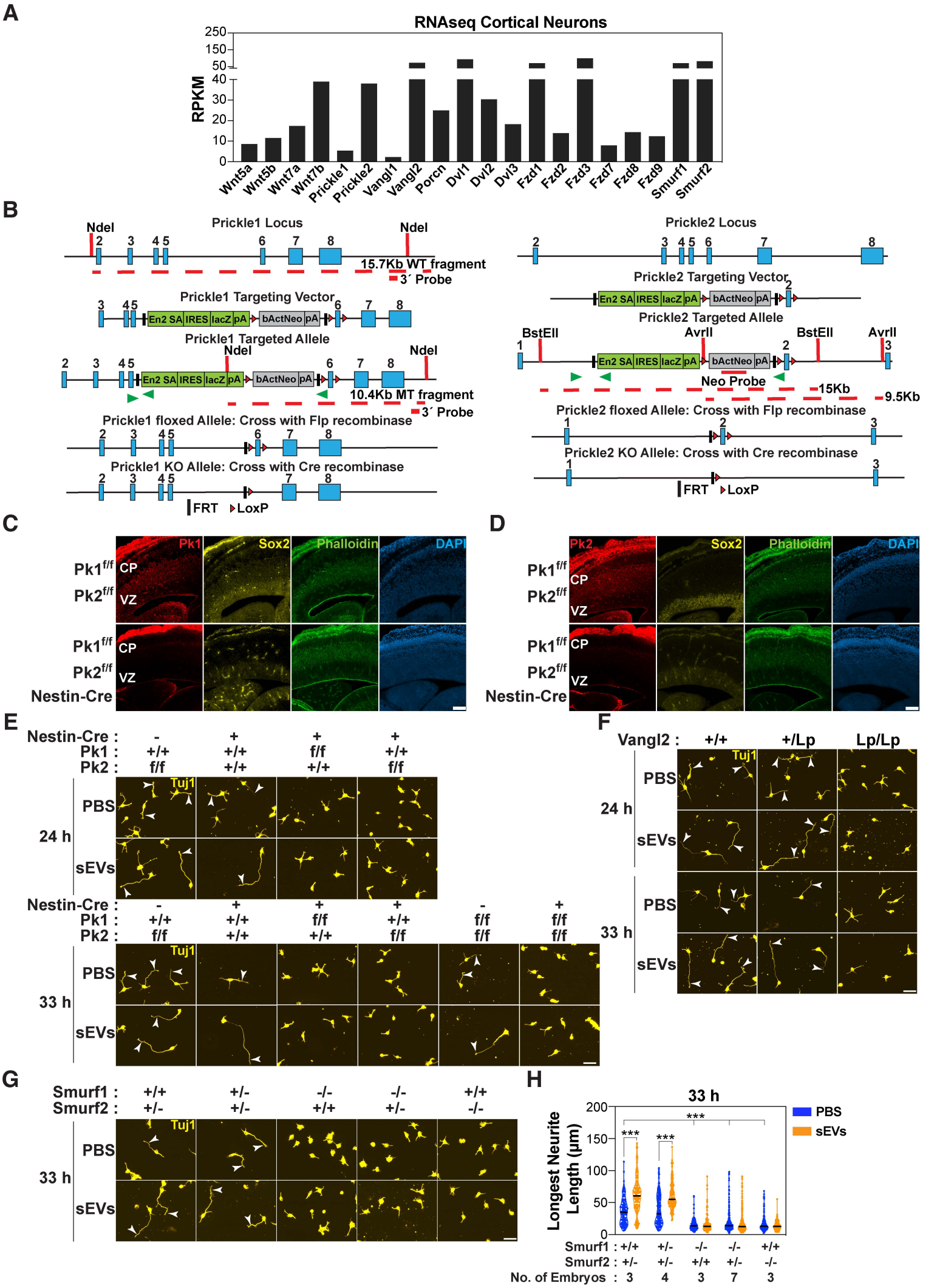
A
RNAseq Cortical Neurons
RPKM
250
150
50
40
30
20
10
0
Wnt5a
Wnt5b
Wnt7a
Wnt7b
Prickle1
Prickle2
Vangl1
Vangl2
Porcn
Dvl1
Dvl2
Dvl3
Fzd1
Fzd2
Fzd3
Fzd7
Fzd8
Fzd9
Smurf1
Smurf2
B
Prickle1 Locus
NdeI
15.7Kb WT fragment
3´ Probe
Prickle1 Targeting Vector
En2 SA
IRES
lacZ
pA
bActNeo
Prickle1 Targeted Allele
10.4Kb MT fragment
Prickle1 floxed Allele: Cross with Flp recombinase
Prickle1 KO Allele: Cross with Cre recombinase
FRT
LoxP
Prickle2 Locus
Prickle2 Targeting Vector
Prickle2 Targeted Allele
BstEII
AvrII
Neo Probe
15Kb
9.5Kb
Prickle2 floxed Allele: Cross with Flp recombinase
Prickle2 KO Allele: Cross with Cre recombinase
C
Pk1
Sox2
Phalloidin
DAPI
Pk1f/f
Pk2f/f
CP
VZ
Nestin-Cre
D
Pk2
E
Nestin-Cre :
Pk1 :
Pk2 :
Tuj1
PBS
sEVs
24 h
33 h
F
Vangl2 :
+/+
+/Lp
Lp/Lp
G
Smurf1 :
Smurf2 :
H
33 h
Longest Neurite Length (µm)
PBS
sEVs
***
No. of Embryos :

Figure S5

Figure S5. The PCP components, Pk1/2 and Vangl2, are required for sEV-induced growth of the longest neurite. Related to Fig. 2. (A) Expression of PCP genes and Wnts in cortical neurons. Total RNA was isolated from E15.5-16.5 cortical neurons after 33 h of *in vitro* culturing. An RNA sequence library was constructed, and high-quality reads were aligned to the *M. musculus* genome and expression of the indicated genes plotted. RPKM, Reads per kilobase of transcript per million mapped reads. (**B)** Schematic maps of the Pk1 and Pk2 wild type allele, targeting vector, targeted allele, floxed allele after crossing with Flp recombinase and knockout allele after crossing with Cre recombinase are shown. Green arrowheads indicate the position of PCR primers for genotyping. **(C, D)** Brain cryosections of E15.5 mouse embryo were stained with antibodies for Pk1 and Sox2 **(C)** or Pk2 and Sox2 **(D)** along with phalloidin. CP: cortical plate, VZ: ventricular zone. Scale bar, 100 μm. **(E-H)** Cortical neurons (E15.5-16.5) were isolated from Pk1 and Pk2 conditional knockout mice **(E)** or Vangl2 mutant littermates **(F)** or Smurf1 and Smurf2 knockout mice **(G, H)**, and treated with sEVs from L cells, 4 h after plating. Neurons were fixed at 24 and 33 h and stained with Tuj1. Representative images are shown. Arrowheads mark the longest neurite. Scale bar, 40 μm. **(H)** The length of the longest neurite was quantified from 30 neurons per embryo, and the total number of embryos analyzed was indicated below the genotypes. Statistical significance: ***$p<0.001$ using two-way ANOVA with Tukey's post-test.

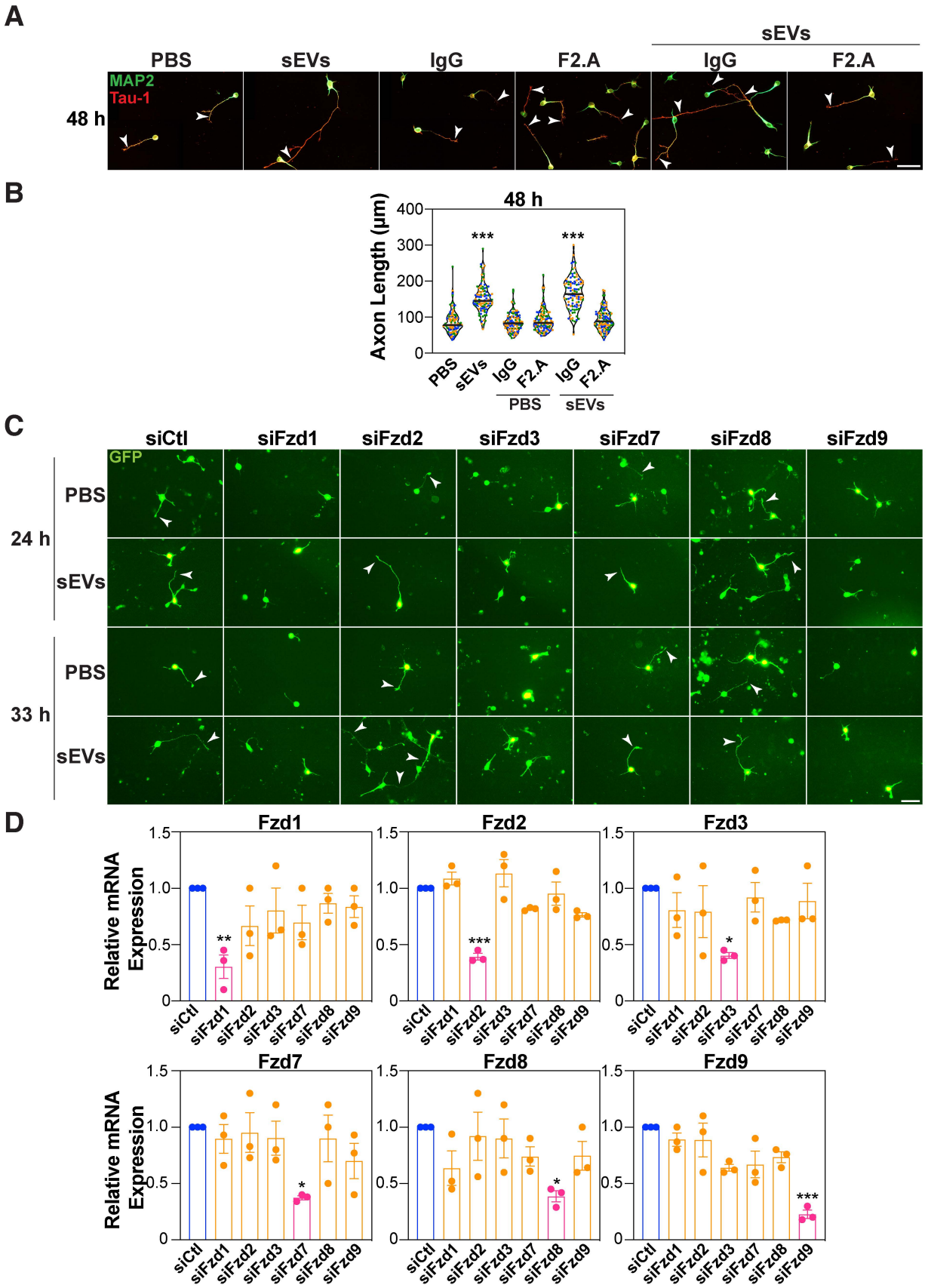
A
sEVs
PBS
sEVs
IgG
F2.A
IgG
F2.A
MAP2
Tau-1
48 h
B
48 h
Axon Length (μm)
400
300
200
100
0
***
***
PBS
sEVs
IgG
F2.A
IgG
F2.A
PBS
sEVs
C
siCtl
siFzd1
siFzd2
siFzd3
siFzd7
siFzd8
siFzd9
GFP
24 h
PBS
sEVs
33 h
PBS
sEVs
D
Fzd1
Fzd2
Fzd3
Fzd7
Fzd8
Fzd9
Relative mRNA Expression
1.5
1.0
0.5
0
**
***
*
*
*
***
siCtl
siFzd1
siFzd2
siFzd3
siFzd7
siFzd8
siFzd9

Figure S6

Figure S6. The PCP components, Fzds, are required for sEV-induced growth of the longest neurite. Related to Fig. 3. (A-B) Dissociated E15.5-16.5 mouse cortical neurons were treated with sEVs (5 µg/mL) from L cells and IgG or a Fzd blocking antibody, F2.A (100 nM), 24 h after plating. Neurons were fixed at 48 h, and neuronal morphology was examined in neurons immunostained for MAP2 (dendrites, green) and Tau-1 (axons, red). Representative images are shown **(A)**. Arrowheads mark Tau-1 positive axons. Scale bar, 50 µm. **(B)** The length of the Tau-1 positive axons was quantified from a minimum of 90 neurons per condition from 3 independent experiments and plotted as a violin plot with values from each experiment distinctly colored and the median marked by a black line. **(C)** Representative images of dissociated E15.5-16.5 cortical neurons electroporated with siRNA against Fzds (siFzds) or siControl (siCtl) along with a GFP-expressing plasmid and then treated with sEVs (5 µg/mL) from L cells, 4 h after plating. Arrowheads mark the longest neurite. Scale bar, 40 µm. **(D)** Knockdown efficiency for Fzds was determined in GFP-positive neurons isolated by FACS. Relative mRNA expression was determined by qPCR and is plotted as the mean ± SEM from 3 independent experiments. Statistical significance: *$p<0.05$, **$p<0.01$, ***$p<0.001$ using one-way ANOVA with Dunnett's post-test.

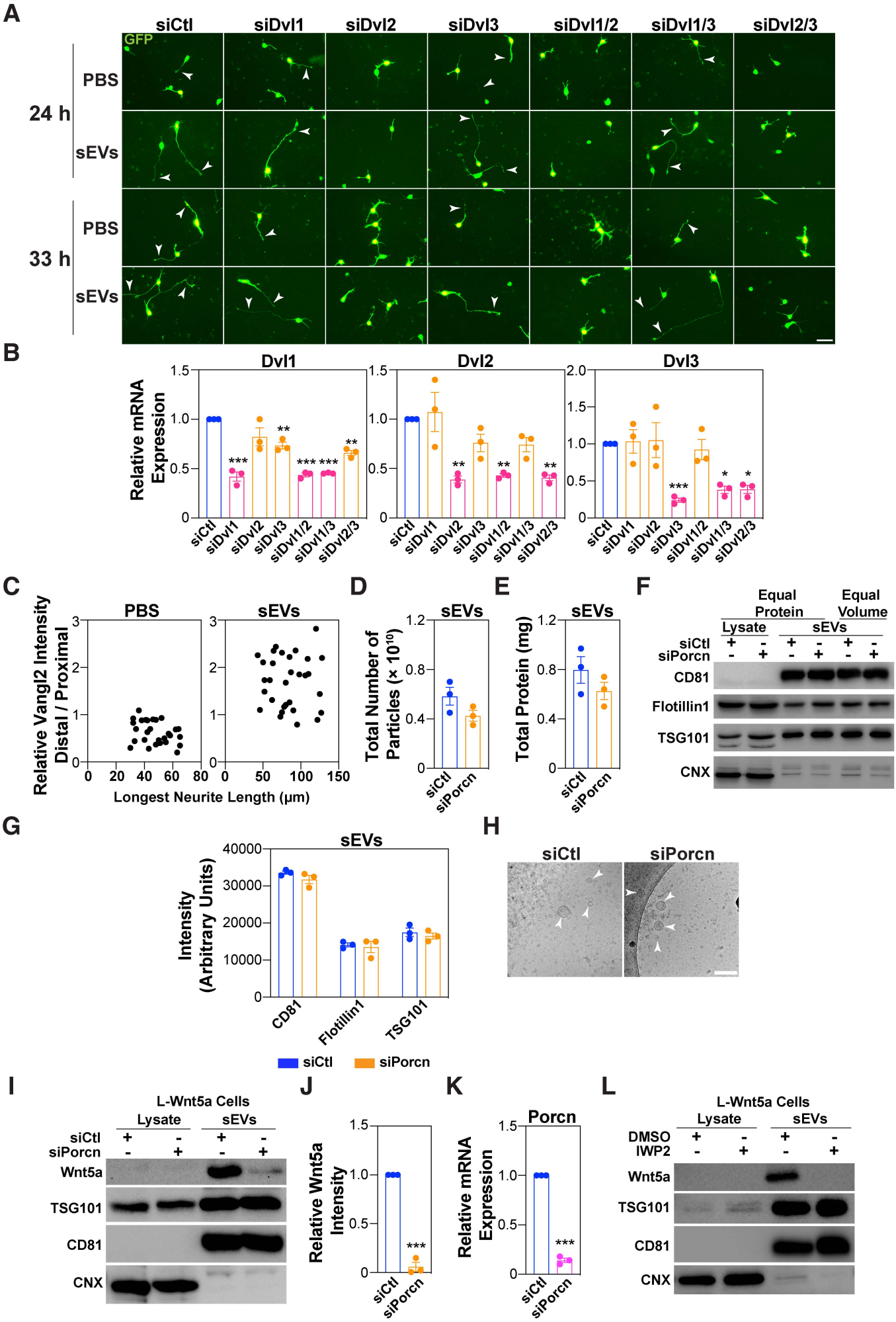
A
siCtl
siDvl1
siDvl2
siDvl3
siDvl1/2
siDvl1/3
siDvl2/3
GFP
24 h
PBS
sEVs
33 h
PBS
sEVs
B
Dvl1
Dvl2
Dvl3
Relative mRNA Expression
C
PBS
sEVs
Relative Vangl2 Intensity Distal / Proximal
Longest Neurite Length (μm)
D
sEVs
Total Number of Particles (× 10^10)
siCtl
siPorcn
E
sEVs
Total Protein (mg)
F
Equal Protein
Equal Volume
Lysate
sEVs
siCtl
siPorcn
CD81
Flotillin1
TSG101
CNX
G
sEVs
Intensity (Arbitrary Units)
CD81
Flotillin1
TSG101
siCtl
siPorcn
H
siCtl
siPorcn
I
L-Wnt5a Cells
Lysate
sEVs
siCtl
siPorcn
Wnt5a
TSG101
CD81
CNX
J
Relative Wnt5a Intensity
siCtl
siPorcn
K
Porcn
Relative mRNA Expression
siCtl
siPorcn
L
L-Wnt5a Cells
Lysate
sEVs
DMSO
IWP2
Wnt5a
TSG101
CD81
CNX

Figure S7

Figure S7. Related to Fig. 3 and 4. (A) Representative images of dissociated E15.5-16.5 cortical neurons electroporated with siRNA against Dvls (siDvls) or siControl (siCtl) along with a GFP-expressing plasmid and then treated with sEVs (5 μg/mL) from L cells, 4 h after plating. Arrowheads mark the longest neurite. Scale bar, 40 μm. **(B)** Knockdown efficiency for Dvls was determined in GFP-positive neurons isolated by FACS. Relative mRNA expression was determined by qPCR and is plotted as the mean ± SEM from 3 independent experiments. (**C**) The ratio of distal/proximal Vangl2 intensity as a function of the longest neurite length in neurons treated with PBS or sEVs is quantified from 30 neurons from 3 independent experiments. (**D**) The total number of particles in the sEV pellet (100,000 x g) were measured using NTA. (**E**) The total amount of protein in the sEV pellet was measured by Bradford assay. (**F**) Characterization of sEVs derived from porcupine-deficient L cells. Representative immunoblot of the cell lysate and 100,000 x g pellet (sEVs) analyzed for EV markers and calnexin (CNX). (**G**) Quantification of **(F)**. sEVs were collected from an equal number of cells, and equal volumes of sEV pellets (right two lanes) were used for comparison. Protein bands were quantified using ImageJ. **(H)** Representative TEM images of sEV pellet. Arrowheads indicate round vesicles. Scale bar, 200 nm. **(I-L)** Porcupine inhibition blocks Wnt5a secretion in sEVs. L-Wnt5a cells were treated with siCtl or siPorcupine (siPorcn) (**I-K**) and DMSO or IWP2 (10 μM) **(L)** followed by isolation of sEVs. A representative immunoblot of sEVs and lysates indicating the level of Wnt5a, EV markers and CNX is shown **(I, L)**. **(J)** Quantification of **(I)**. Protein bands were quantified using ImageJ. **(K)** Knockdown efficiency of Porcupine in L-Wnt5a cells.

Values are plotted as the mean ± SEM from 3 independent experiments **(B, D, E, G, K, L)**. Statistical significance: *$p<0.05$, **$p<0.01$, ***$p<0.001$ using unpaired t-test **(D, E, K, L)**, one-way ANOVA with Dunnett's post-test **(B)**, or two-way ANOVA with Tukey's post-test **(G)**.

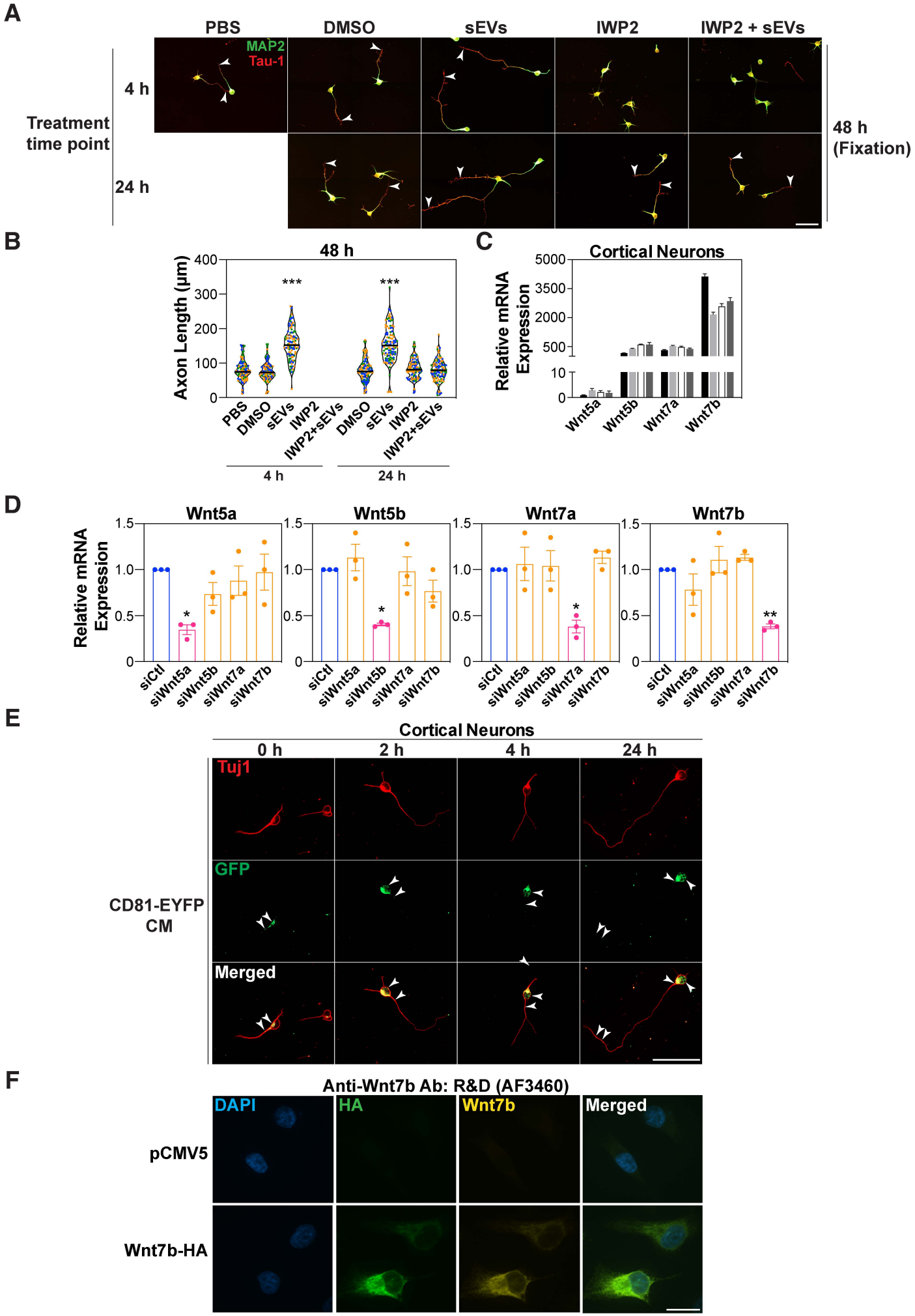
A
PBS
DMSO
sEVs
IWP2
IWP2 + sEVs
MAP2
Tau-1
Treatment time point
4 h
24 h
48 h (Fixation)
B
48 h
Axon Length (µm)
400
300
200
100
0
***
***
PBS
DMSO
sEVs
IWP2
IWP2+sEVs
DMSO
sEVs
IWP2
IWP2+sEVs
4 h
24 h
C
Cortical Neurons
Relative mRNA Expression
5000
3500
2000
500
10
0
Wnt5a
Wnt5b
Wnt7a
Wnt7b
D
Wnt5a
Wnt5b
Wnt7a
Wnt7b
Relative mRNA Expression
1.5
1.0
0.5
0
*
*
*
**
siCtl
siWnt5a
siWnt5b
siWnt7a
siWnt7b
E
Cortical Neurons
0 h
2 h
4 h
24 h
Tuj1
GFP
Merged
CD81-EYFP CM
F
Anti-Wnt7b Ab: R&D (AF3460)
DAPI
HA
Wnt7b
Merged
pCMV5
Wnt7b-HA

Figure S8

Figure S8. Related to Fig. 4 and 5. (A-B) Dissociated E15.5-16.5 mouse cortical neurons were treated with sEVs (5 μg/mL) from L cells and DMSO or IWP2 (10 μM), 4 h or 24 h after plating. Neurons were fixed at 48 h, and neuronal morphology was examined in neurons immunostained for MAP2 (dendrites, green) and Tau-1 (axons, red). Representative images are shown **(A)**. Arrowheads mark Tau-1 positive axons. Scale bar, 50 μm. **(B)** The length of the Tau-1 positive axons was quantified from a minimum of 90 neurons per condition from 3 independent experiments and plotted as a violin plot with values from each experiment distinctly colored and the median marked by a black line. For IWP2-treated neurons at 4 h, a comparable number of data points were not available due to lack of Tau-1 positive axons. **(C)** Expression of Wnts in cortical neurons. RNA was isolated from cortical neurons at 0, 12, 24 and 33 h of culturing. A representative plot indicating mRNA expression relative to Wnt5a, determined by qPCR from 2 independent experiments is shown. **(D)** Efficiency of siRNA-mediated knockdown of Wnts. RNA was isolated from GFP-positive neurons after FACS. Relative mRNA expression was determined by qPCR. **(E)** sEVs can be internalized by neurons. Cortical neurons were treated with 10X concentrated conditioned media (CM) from L cells stably expressing CD81-EYFP, 24 h after plating for 30 min. Neurons were washed and subsequently treated with regular complete media for 0, 2, 4 and 24 h. Representative images of neurons immunostained with GFP and Tuj1 from 30 neurons from 3 independent experiments are shown. Arrowheads indicate the localization of sEVs. Scale bar, 40 μm **(F)** Wnt7b antibody characterization. MDA-MB-231 cells were transfected with 2 μg of either pCMV5 control or C-terminal HA-tagged Wnt7b (Wnt7b-HA). Cells were fixed after 48 h and immunostained with HA (green) and Wnt7b (yellow) antibodies. Scale bar, 20 μm.

Statistical Significance: *$p<0.05$, **$p<0.01$, ***$p<0.001$ using one-way ANOVA with Dunnett's post-test **(B, D)**.

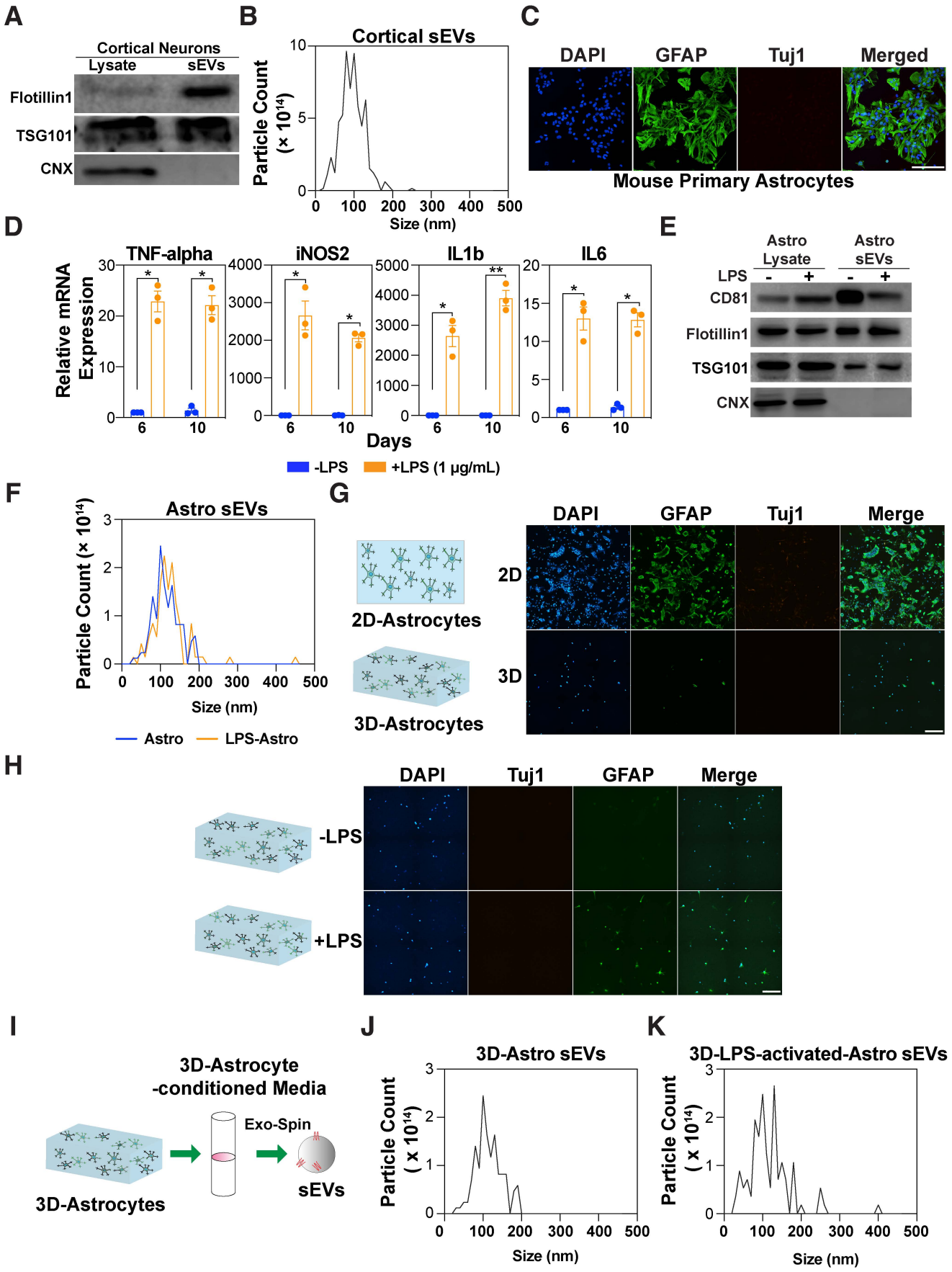
A
Cortical Neurons
Lysate
sEVs
Flotillin1
TSG101
CNX
B
Cortical sEVs
Particle Count (× 10^14)
Size (nm)
C
DAPI
GFAP
Tuj1
Merged
Mouse Primary Astrocytes
D
TNF-alpha
iNOS2
IL1b
IL6
Relative mRNA Expression
Days
-LPS
+LPS (1 μg/mL)
E
Astro Lysate
Astro sEVs
LPS
CD81
Flotillin1
TSG101
CNX
F
Astro sEVs
Particle Count (× 10^14)
Size (nm)
Astro
LPS-Astro
G
2D-Astrocytes
3D-Astrocytes
DAPI
GFAP
Tuj1
Merge
2D
3D
H
DAPI
Tuj1
GFAP
Merge
-LPS
+LPS
I
3D-Astrocyte -conditioned Media
Exo-Spin
3D-Astrocytes
sEVs
J
3D-Astro sEVs
Particle Count (x 10^14)
Size (nm)
K
3D-LPS-activated-Astro sEVs
Particle Count (x 10^14)
Size (nm)

Figure S9

Figure S9. Related to Fig. 6. (A) Immunoblot of sEVs and lysates from cortical neurons. **(B)** NTA of the sEV pellet. **(C)** Purity of primary astrocytes cultures. Enriched cultures of astrocytes from P1-P4 mouse pups were immunostained for the astrocyte marker, GFAP, and the neuronal marker Tuj1. Scale bar, 200 µm. **(D)** LPS activates mouse primary astrocytes. Astrocytes were treated with LPS (1 µg/mL), and RNA was isolated after 6 or 10 days. Relative expression of pro-inflammatory genes was measured by qPCR. **(E)** Immunoblot of lysates and the sEV pellet from primary astrocytes. **(F)** NTA of the sEV pellet. **(G)** Astrocytes are activated upon culturing in 2D plates. Representative immunofluorescence images of astrocytes grown either on a glass surface or in a soft collagen gel. Scale bar, 200 µm. **(H)** LPS activates astrocytes grown in 3D-collagen gels. Astrocytes were treated with LPS (1 µg/mL), fixed after 48 h and subsequently immunostained with GFAP and Tuj1 antibodies. Representative images are shown. Scale bar, 200 µm. **(I)** A schematic representation of sEV purification from astrocytes grown in a soft 3D-collagen gel. CM was collected after 6 days and subsequently sEVs were purified using Exo-spin^{TM} columns. **(J and K)** NTA of the sEVs.

NTA plots are from 1 representative experiment out of 3 independent purifications **(B, F, J, K)**. Values are plotted as the mean ± SEM from 3 independent experiments **(D)**. Statistical significance: *$p<0.05$, **$p<0.01$ using two-way ANOVA with Tukey's post-test **(D)**.

Table S1: Genotyping primers

Gene	Primers
Pk1-F	CAGACTCCTGTCAACGCGATG
Pk1-R	CGCCTGCACAACAGCACTGTC
Pk1-MT-R	CCCCACAACGGGTTCTTCTGTTAG
Pk2-F	TGTGGCCACATTTGTTTTAGAGG
Pk2-R	CACACACTAACCAGAAATATCATC
Pk2-MT-R	CCCCACAACGGGTTCTTCTGTTAG
Vangl2	TGGCTGTCTTCTGCACTCAC
Vangl2-R	GCACCTTCTTGGTGCTCACT
Smurf1-F	CAGATGCTGAGGCAGGAGAATCATGAG
Smurf1-R	CAGTCCCCTCCCAACACACAATCAC
Smurf1-MT-R	AGTTCTAATTCCATCAGAAGCTGACTCTAG
Smurf2-F	TGCTATGGCTTCTGACTATTAAAAGGTC
Smurf2-R	CTTAAACATCAGCTCCTGAGTACACAAC
Smurf2-MT-R	AGTTCTAATTCCATCAGAAGCTGACTCTAG
Cre-F	TGACCGTACACCAAAATTTG
Cre-R	ATTGCCCCTGTTTCACTATC

Table S2: List of siRNAs

Gene	Dharmacon Catalog #
Dvl1	D-040910-01, D-040910-02, D-040910-03, D-040910-04
Dvl2	D-040921-01, D-040921-02, D-040921-03, D-040921-04
Dvl3	D-040922-01, D-040922-02, D-040922-03, D-040922-04
Frizzled1	D-063230-01, D-063230-02, D-063230-03, D-063230-04
Frizzled2	D-040443-01, D-040443-02, D-040443-03, D-040443-04
Frizzled3	D-048416-01, D-048416-02, D-048416-03, D-048416-04
Frizzled7	D-041631-01, D-041631-02, D-041631-03, D-041631-04
Frizzled8	D-045544-01, D-045544-02, D-045544-03, D-045544-04
Frizzled9	D-040416-01, D-040416-02, D-040416-03, D-040416-04
Prickle1	D-042729-01, D-042729-02, D-042729-03, D-042729-04
Prickle2	D-056882-01, D-056882-02, D-056882-05, D-056882-06
Vangl1	D-057276-01, D-057276-02, D-057276-03, D-057276-04
Vangl2	D-059396-01, D-059396-02, D-059396-03, D-059396-17
Wnt5a	D-065584-01, D-065584-02, D-065584-03, D-065584-04
Wnt5b	D-060428-01, D-060428-03, D-060428-04, D-060428-17
Wnt7a	D-058932-02, D-058932-03
Wnt7b	D-042139-01, D-042139-02, D-042139-03, D-042139-04
Porcupine	D-049203-01, D-049203-02, D-049203-03, D-049203-04
Wls	D-060922-01, D-060922-02, D-060922-03, D-060922-04

Table S3: List of antibodies

Reagent or Resource	Source	Identifier
Antibodies		
Mouse anti-MAP-2 (Clone AP20, 1:500)	Millipore	MAB3418
Mouse anti-Tubulin β 3 (Clone Tuj1, 1:3000)	Biolegend	801202
Mouse anti-Tau-1 (Clone PC1C6, 1:300)	Millipore	MAB3420
Mouse anti-TSG101 (1:1500)	GeneTex	GTX70255
Mouse anti-Flotillin-1 (1:1500)	BD Transduction	618021
Mouse anti-CD81 (B-11, 1:1500)	Santa Cruz	sc-166029
Mouse anti-Prickle1 (F-5, 1:100)	Santa Cruz	Sc-393034
Mouse anti-Prickle2 (Clone 3B4.1, 1:100)	Millipore	MABN1529
Rabbit anti-GFAP (1:500)	Dako	Z0334
Rabbit anti-GFP (1:400)	Invitrogen	A11122
Rabbit anti-β III Tubulin (1:500)	Abcam	ab18207
Rabbit anti-Calnexin (1:2000)	(Jackson *et al*, 1994)[1]	N/A
Rat anti-Vangl2 (Clone 2G4, 1:200)	Millipore	MABN750
Rat anti-HA (1:1000)	Roche	11867423001
Goat anti-Wnt7b (1:200)	R&D Systems	AF3460
Goat anti-Wnt5a (1:1000)	R&D Systems	AF645
Goat anti-GFP (1:1000)	Rockland	600-101-215
Donkey anti-goat DyLight™ 488 (1:1000)	Thermo Fisher Scientific	SA5-10086
Donkey anti-goat Alexa Fluor™ 647 (1:1000)	Thermo Fisher Scientific	A21447
Goat anti-Mouse Alexa Fluor® 488 (1:1000)	Invitrogen	A11029
Goat anti-Rabbit Alexa Fluor® 488 (1:1000)	Invitrogen	A11034
Goat anti-Mouse Alexa Fluor™ 488 (1:500)	Thermo Fisher Scientific	A21121
Goat anti-Rat Alexa Fluor™ 488 (1:1000)	Thermo Fisher Scientific	A11006
Goat anti-Mouse Alexa Fluor™ 568 (1:500)	Thermo Fisher Scientific	A21134
Goat anti-Mouse Alexa Fluor® 594 (1:1000)	Invitrogen	A11032
Goat anti-Rabbit Alexa Fluor® 594 (1:1000)	Invitrogen	A11012
Goat anti-rabbit Alexa Fluor™ 647 (1:1000)	Thermo Fisher Scientific	A21244
Donkey anti-Goat IgG-HRP (1:5000)	Jackson ImmunoResearch	705-035-147
Donkey anti-Mouse IgG-HRP (1:5000)	Jackson ImmunoResearch	715-035-150
Donkey anti-Rabbit IgG-HRP (1:5000)	Jackson ImmunoResearch	711-035-152
IgG F2.A	(Pavlovic *et al.*, 2018)[2]	N/A
IgG	(Enderle *et al*, 2021)[3]	N/A

[1]Jackson MR, Cohen-Doyle MF, Peterson PA, Williams DB (1994) Regulation of MHC class I transport by the molecular chaperone, calnexin (p88, IP90). Science 263: 384-387.

[2]Pavlovic Z, Adams JJ, Blazer LL, Gakhal AK, Jarvik N, Steinhart Z, Robitaille M, Mascall K, Pan J, Angers S *et al* (2018) A synthetic anti-Frizzled antibody engineered for broadened specificity exhibits enhanced anti-tumor properties. *MAbs* 10: 1157-1167.

[3]Enderle L, Shalaby KH, Gorelik M, Weiss A, Blazer LL, Paduch M, Cardarelli L, Kossiakoff A, Adams JJ, Sidhu SS (2021) A T cell redirection platform for co-targeting dual antigens on solid tumors. *MAbs* 13: 1933690.

Table S4: Primers for gene expression analysis

qPCR Primers		
Gene	**Forward Primer**	**Reverse Primer**
Wnt3a	CTCCTCTCGGATACCTCTTAGTG	GCATGATCTCCACGTAGTTCCTG
Wnt5a	CAACTGGCAGGACTTTCTCAA	CATCTCCGATGCCGGAACT
Wnt5b	CTGCTGACTGACGCCAACT	CCTGATACAACTGACACAGCTTT
Wnt7a	GGTGCGAGCATCATCTGTAA	CATTTGGGAGCCTTCTCCTATG
Wnt7b	GGATGCCCGTGAGATCAAA	GACACACCGTGACACTTACA
Prickle1	TCCCGAAACAAGGTCAGATTTA	TCTCTGGATCTGGCTGACT
Prickle2	CACTGCTTTGAGTCCCTGTATG	TCTGTAGCATGCCAGTGTTG
Vangl1	GCTGGCCTGAAAGTCTACAA	CGTGTTCGGCCTCTTCATAATA
Vangl2	ACTCGGGCTATTCCTACAAGT	TGATTTATCTCCACGACTCCCAT
Frizzled1	GCTGAGCTTGGAACTTTGTG	AGCCTCCAGCAACCAAA
Frizzled2	GCCGTCCTATCTCAGCTATAAGT	TCTCCTCTTGCGAGAAGAACATA
Frizzled3	ATGGCTGTGAGCTGGATTGTC	GGCACATCCTCAAGGTTATAGGT
Frizzled7	ATATCACGGCGAGAAAGGC	GCAGGATGGTCTGGTTGTAG
Frizzled8	ATGGAGTGGGGTTACCTGTTG	CACCGTGATCTCTTGGCAC
Frizzled9	TCCGCGTTGTGTTTCTTCT	GGCCAAGGAGTAGACATTGTAG
Dvl1	GAAGTCAGGCTTCAGCTGTT	CTACCTGTAAGTTCTGGAGGGA
Dvl2	CCATCCTTCCACCCTAATGTATC	CCATGTTCACTGCTGTCTCT
Dvl3	TGGTTTCATCCGCCATACC	ATCATGGTCGTGAAGCGATAG
Cd81	GTACCTGGAACTGGGAAACAA	CCCAGGAAGCCTACAAACAT
Smpd2	CAAAGGCTATCGCTCACCTATC	CTGGATTGGGTGTTTGGAGAA
Wntless	TGGGAAGCAGTCTAGCCTCC	GCAGCACAAGCCAAGGTGATA
Porcupine	GAGAAGGACCACCTGGAATG	ATAAGACATGGGCAGGTTCC
iNOS2	GGCAGCCTGTGAGACCTTTG	GCATTGGAAGTGAAGCGTTTC
IL1b	CAGGCAGGCAGTATCACTCA	TGTCCTCATCCTGGAAGGTC
IL6	ATGGATGCTACCAAACTGGAT	TGAAGGACTCTGGCTTTGTCT
TNF-α	ACGGCATGGATCTCAAAGAC	GTGGGTGAGGAGCACGTAGT
Gapdh	AGGTCGGTGTGAACGGATTTG	TGTAGACCATGTAGTTGAGGTCA